TABLE 3. Characteristics of HBV/HIV-1-coinfected patients

Characteristic	Value[a] for genotype:			*P*
	All (n = 26)	A (n = 21)	C (n = 5)	
Age (yr)	34 (30–37)	33 (29–37)	56 (46–57)	<0.01
Suspected route of HIV-1 infection	MSM	MSM	MSM	
AST (IU/liter)	31 (26–63)	29 (26–48)	54 (20–74)	
ALT (IU/liter)	43 (33–90)	42 (32–85)	44 (34–99)	
No. HBcAg IgM positive	9	9	0	<0.01
CD4 (/μl)	293 (91–492)	300 (94–484)	202 (9–494)	
HIV-1viral load (copies/ml)	6.4×10^4 (2.0×10^4–2.0×10^5)	6.8×10^4 (2.4×10^4–2.1×10^5)	2.4×10^4 (2.4×10^3–9.7×10^4)	
HBV viral load (copies/ml)	4.4×10^8 (4.9×10^4–6.3×10^8)	6.3×10^8 (4.7×10^4–6.3×10^8)	2.0×10^8 (4.7×10^5–6.3×10^8)	

[a] Median values are shown. Numbers in parentheses represent interquartile ranges.

second most predominant HBV genotype in Japan, was not detected in our study. Interestingly, the genotype A and C populations showed obvious differences in genetic diversity. The 21 group A2 samples (Fig. 3) formed a cluster with little

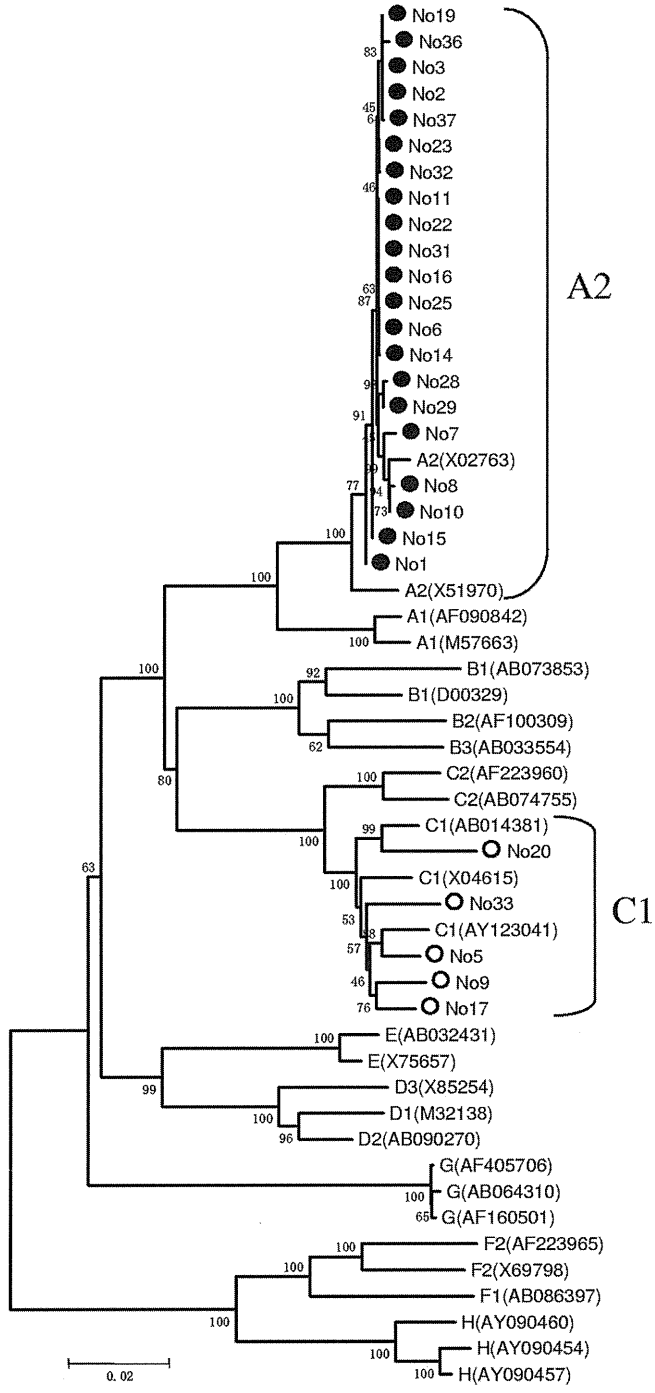

FIG. 3. Phylogenetic tree analyses of HBV isolated from HBV/HIV-1-coinfected patients. The phylogenetic tree was constructed using 26 full-length HBV genome sequences detected in HBV/HIV-1-coinfected patients in Nagoya (both solid and open circles) and 23 reference sequences from the NCBI database. Twenty-one and five cases were distributed in the clusters of genotype A (solid circles) and C (open circles), respectively.

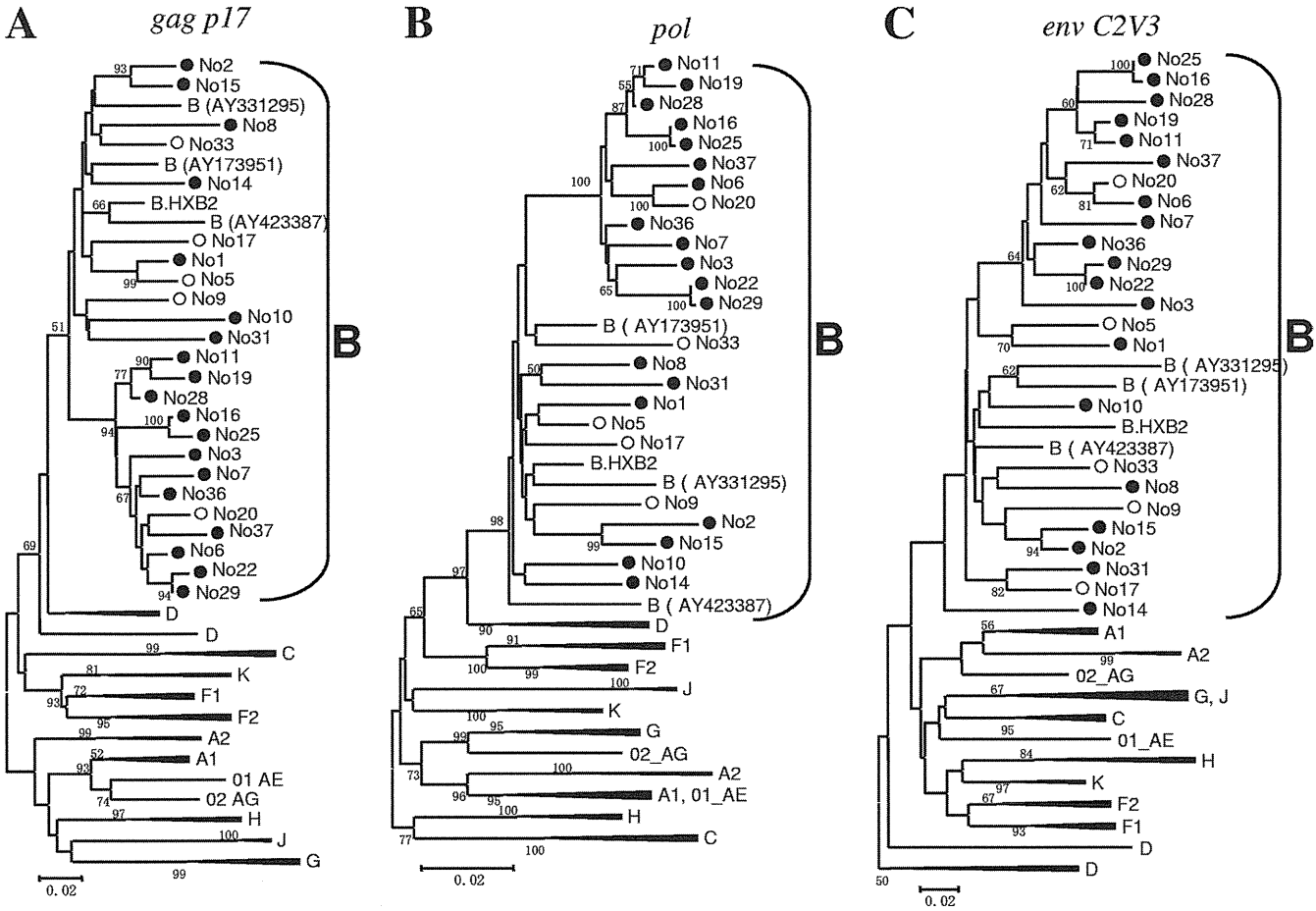

FIG. 4. Phylogenetic tree analyses of HIV-1 isolated from HBV/HIV-1-coinfected patients. Phylogenetic trees were constructed using the 25 HIV-1 sequences obtained in this study and 62 HIV-1 reference sequences from the Los Alamos National Laboratory database. The nucleotide base sequences of *gag p17* (A), *pol* PR to RT (B), and *env C2V3* (C) gene regions were analyzed. In all analyses, all the HIV-1-positive cases detected in Nagoya (both solid and open circles) were distributed in the subtype B cluster. Cases of coinfection with genotype C HBV are shown with open circles.

or no genetic distance between each other, indicating their extremely close genetic relationships. In contrast, the five group C1 cases did not form a single cluster and had longer branches than those of group A2.

Patients with genotypes A and C also differed significantly in age (Table 3). The median age of the genotype A patients was 33 years (IQR, 29 to 37), whereas that of the genotype C patients was 56 (IQR, 46 to 57) ($P < 0.01$). Furthermore, all nine HBcAg IgM-positive cases, including five suspected cases of acute infection, were categorized in genotype A2, suggesting ongoing active transmission of the virus among the Japanese MSM population. Thus, the genotype A2 population appeared to be younger, with more acute cases, and infected with an almost genetically identical HBV strain. These two genotypes did not differ significantly in regard other clinical data, such as AST and ALT levels, $CD4^+$ T cell count, and HBV and HIV-1 viral loads.

To clarify the detailed epidemiological features of HBV/HIV-1-coinfected patients, the HIV-1 subtypes and their genetic distances were determined by phylogenetic analyses of three genome regions, *gag p17*, *pol*, and *env C2V3*. All 26 samples were determined as subtype B (Fig. 4A, B, and C), and interestingly, branch patterns and relationships among cases were different from those for HBV. There were six paired cases, demonstrating a significantly close genetic relationship (>50% bootstrap value) in more than two regions. These paired cases were cases 1 and 5, 2 and 15, 6 and 20, 11 and 19, 16 and 25, and 22 and 29, and these connections were not evident in the HBV phylogeny, suggesting different origins of sexual partner between the two pathogens in each pair. An alternative explanation could be that little genetic variation in HBV made it difficult to clarify the genetic relationships between cases. However, there was one discordant pair (cases 1and 5); one case had HBV genotype A, and the other case had HBV genotype C2. Furthermore, the other four HBV genotype C2 cases (cases 9, 17, 20, and 33) were scattered among HIV-1 phylogenies within genotype B HIV-1-infected patients.

HBV strains detected in HIV-1-infected patients from Nagoya are the same viruses found in other parts of Japan. To clarify whether the dominance of genotype A HBV in HIV-1-infected MSM is a regional issue in the Nagoya urban area or a more nationwide epidemic, we reconstructed an HBV phylogenetic tree of 26 cases together with HBV sequences col-

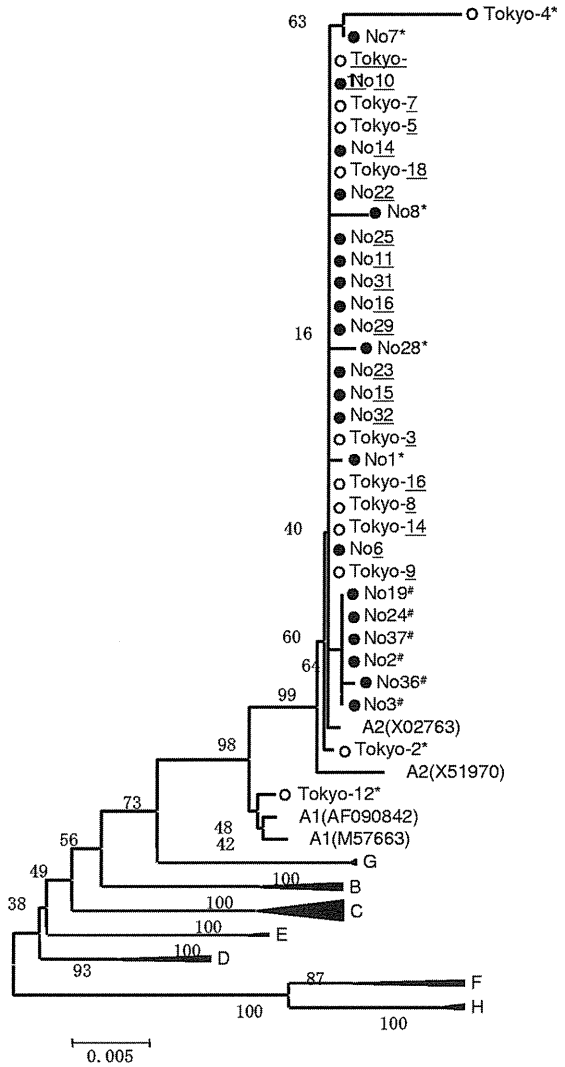

FIG. 5. Phylogenetic tree analysis of 35 HBV region S sequences, 22 from Nagoya (solid circles) and 13 from Tokyo (open circles). Three genetically different groups are indicated by asterisks, pound signs, and underlining.

lected at a different time and from a different area of Japan, i.e., 12 genotype A sequences from HBV/HIV-1-coinfected patients collected in Tokyo about 10 years before this study (8). As no full genome sequences were available for the Tokyo cases, only the S gene (681 bp [bp 155 to 835]) was analyzed. From the phylogenetic tree pattern, genotype A was classified into three groups (Fig. 5). The first is a group of 21 identical sequences (underlined in Fig. 5). As this group had the largest number of cases and included sequences from both Nagoya and Tokyo, this strain appears to be prevailing nationwide. The second group is a cluster of cases, i.e., cases 2, 3, 19, 24, 36, and 37. As all six cases were from Nagoya, this isolate still seems to be in an endemic status. The third group comprises isolates with longer branches (noted by asterisks), i.e., Tokyo-2, -4, and -12 and Nagoya-1, -7, -8, and -28. These isolates appear to be quite distinct from the others, suggesting that their origin may not be sexual contact but another route, such as MTCT or transfusions.

The prevailing HBV genotype A2 emerged more recently than most other genotypes. To estimate the emergence time of the prevailing genotype A2 strain, we estimated its mutation rate per year and tMRCA. First, the median mutation rate per year was calculated as 3.23×10^{-5} (5.62×10^{-8} to 9.01×10^{-5}), which is close to those previously reported (10, 18). Next, the median tMRCAs of all A strains, A1, A2, and C were determined to be 370.8, 88.9, 184.3, and 494.9 years ago, respectively (Table 4; Fig. 6). Thus, the A2 genotype is one of the youngest HBV genotypes.

A lamivudine resistance amino acid HBV mutation detected in an antiretroviral therapy-naïve patient. We clarified not only HBV genotypes but also the incidence of transmitted drug-resistant HBV among the study patients. Analysis of the amino acid sequence of the HBV RT region showed a combined triple amino acid mutation, rtV173L + rtL180M + rtM204V, which was a mutation causing resistance against lamivudine and its 5-fluoro analogue (2′,3′-dideoxy-3′-thia-5-fluorocytidine), in two patients (patients 5 and 8). However, one patient (patient 5) had been treated with stavudine-lamivudine-efavirenz at the time of sample collection, and thus only one case (case 8) was suspected to be a transmitted HBV drug-resistant case. No HIV-1 drug-resistant virus transmission was detected in the study sample.

DISCUSSION

This molecular epidemiological study of HBV infection in HIV-1-seropositive patients revealed epidemiological characteristics that were unique compared to those of the general population in Japan. All HBV/HIV-1-coinfected patients were MSM, they had a 10-fold-higher prevalence (7.9%) than that of the general population, and genotype A was the predominant HBV genotype (31). This distinct HBV epidemic in MSM was first reported in 2001 in other regions of the country (9, 36), a decade before our study. Furthermore, phylogenetic analysis of sequences from the two studies, collected in different regions and years, revealed that an identical genotype A strain prevails among the MSM population nationwide.

Considering the status of HBV epidemiology in the general population of Japan, genotypes C and B must have an equal or greater chance to disseminate among the HIV-1-seropositive

TABLE 4. Estimated times of the most recent ancestor (tMRCAs) for HBV genotypes

Genotype	Mean tMRCA (yr before)		95% HPD[a]	
	Mean	Median	L	H
A	1,294.2	370.8	27.1	4,046.4
A1	306.6	88.9	12.4	976.4
A2	597.4	184.3	18.8	1,886.2
B	345.8	88.5	4.2	1,069.3
C	1,655.3	494.9	36.6	5,124.7
C2	1,062.4	308.6	20.8	3,296.6
D	827.2	226.6	11.2	2,469.4
E	163.7	38.9	4.5	539.7
F	1,060.8	308.2	13.7	3,277.4
H	433.8	110.1	5.6	1,303.0

[a] HPD, highest posterior density.

FIG. 6. Maximum clade credibility tree depicted according to median tMRCA. Nodes with open circles are evaluated points for each genotype summarized in Table 2.

MSM population. In fact, we found five genotype C patients in our study sample, and all five patients were MSM. However, because these five genotype C patients were older and their isolates had longer branches in phylogenetic analysis than the prevailing genotype A isolates, they appear to have been independently infected through either MTCT or blood transfusion events rather than sexual contact. Furthermore, as all five cases were singletons without any genetically close isolates among the samples analyzed, this genotype appeared to be less efficiently transmitted by sexual contact.

Interestingly, predominant genotype A HBV coinfection in HIV-seropositive MSM populations has also been reported in European and South American countries (20, 26, 33), suggesting that the prevailing genotype A in HIV-seropositive MSM has become a worldwide HBV epidemic. Regarding HBV genotypes in the HIV-negative population in Japan, genotype A has been increasing, but the major HBV genotype is still C, with genotype A remaining at 3.5% nationwide and 2.1% in the Tokai area, which includes Nagoya city (9). Therefore, the prevalence of genotype A HBV in the MSM population is significantly higher than in the rest of the population.

Thus, it is interesting to discuss the virological advantages disposing this genotype A isolate to become the major player in HBV/HIV-1 coinfection among MSM. One such advantage might be the higher progression rate (16 to 23%) to chronicity of genotype A than of genotype C (28, 30), enhancing its capacity to serve as a source of new infections. As 9 of 26 genotype A-infected patients (35%) were HBcAg IgM positive and 2 had acute hepatitis, it is obvious that genotype A infections are actively ongoing among the MSM population. Though further studies are needed, considering the tMRCA of the prevailing strain A2, the younger age of patients infected with this strain than of those infected with other genotypes,

and its high prevalence among MSM, this strain may have acquired higher infectivity and efficient transmission through sexual contact.

Another issue we wanted to clarify in this study was the transmission of antiviral drug resistance. We found no antiretroviral resistance in the 26 sequenced cases. On the other hand, we detected two cases with a mutation combination of rtV173L + rtL180M + rtM204V in HBV reverse transcriptase, demonstrating resistance against lamivudine-emtricitabine. One patient was antiretroviral therapy naïve; thus, transmission of drug-resistant HBV is strongly suspected. It is peculiar that the isolate harboring the drug-resistant mutations in HBV was a singleton, considering that genetically identical isolates were prevailing, that there were very low mutation rates that suggest few chances of reverting to wild type, and that there were actively ongoing *de novo* infections. This finding might be due to resistant viruses being masked by wild-type viruses under untreated conditions, as reported in the case of HIV-1 drug resistance (6). The possibility of minority resistance populations of HBV could be verified by detection with a highly sensitive method.

In conclusion, we clarified the molecular epidemiology of HBV/HIV-1 coinfection in Japan. Our data suggest that ongoing HBV infections lie outside prevention programs targeting the MTCT and blood transfusion infection routes, and they suggest the urgent need for new prevention strategies focusing on the high-risk group of the HIV-1-seropositive MSM population.

ACKNOWLEDGMENTS

This study was supported by a Research Grant for Research on HIV/AIDS from the Ministry of Health, Labor, and Welfare of Japan (no. H19-AIDS-007, H21-AIDS-005, and H22-AIDS-004).

We thank Yasuhito Tanaka, Nagoya City University Graduate School of Medical Sciences, for helpful discussion and Claire Baldwin for help in preparing the manuscript.

REFERENCES

1. **Allen, M. I., et al.** 1998. Identification and characterization of mutations in hepatitis B virus resistant to lamivudine. Lamivudine Clinical Investigation Group. Hepatology **27:**1670–1677.
2. **Angus, P., et al.** 2003. Resistance to adefovir dipivoxil therapy associated with the selection of a novel mutation in the HBV polymerase. Gastroenterology **125:**292–297.
3. **Drummond, A. J., S. Y. Ho, M. J. Phillips, and A. Rambaut.** 2006. Relaxed phylogenetics and dating with confidence. PLoS Biol. **4:**e88.
4. **Drummond, A. J., and A. Rambaut.** 2007. BEAST: Bayesian evolutionary analysis by sampling trees. BMC Evol. Biol. **7:**214.
5. **Gatanaga, H., et al.** 2007. Drug-resistant HIV-1 prevalence in patients newly diagnosed with HIV/AIDS in Japan. Antiviral Res. **75:**75–82.
6. **Harrigan, P. R., S. Bloor, and B. A. Larder.** 1998. Relative replicative fitness of zidovudine-resistant human immunodeficiency virus type 1 isolates in vitro. J. Virol. **72:**3773–3778.
7. **Johnson, V. A., et al.** 2009. Update of the drug resistance mutations in HIV-1: December 2009. Top. HIV Med. **17:**138–145.
8. **Koibuchi, T., et al.** 2001. Predominance of genotype A HBV in an HBV-HIV-1 dually positive population compared with an HIV-1-negative counterpart in Japan. J. Med. Virol. **64:**435–440.
9. **Matsuura, K., et al.** 2009. Distribution of hepatitis B virus genotypes among patients with chronic infection in Japan shifting toward an increase of genotype A. J. Clin. Microbiol. **47:**1476–1483.
10. **Michitaka, K., et al.** 2006. Tracing the history of hepatitis B virus genotype D in western Japan. J. Med. Virol. **78:**44–52.
11. **Miyakawa, Y., and M. Mizokami.** 2003. Classifying hepatitis B virus genotypes. Intervirology **46:**329–338.
12. **Norder, H., et al.** 2004. Genetic diversity of hepatitis B virus strains derived worldwide: genotypes, subgenotypes, and HBsAg subtypes. Intervirology **47:**289–309.
13. **Noto, H., et al.** 2003. Combined passive and active immunoprophylaxis for preventing perinatal transmission of the hepatitis B virus carrier state in Shizuoka, Japan during 1980–1994. J. Gastroenterol. Hepatol. **18:**943–949.
14. **Nylander, J.** 2004. MrModeltest v2. Uppsala University, Uppsala, Sweden.
15. **Oda, T.** 2000. Further decline of hepatitis B surface antigen (HBsAg) prevalence in Japan. Jpn. J. Cancer Res. **91:**361.
16. **Okada, K., I. Kamiyama, M. Inomata, M. Imai, and Y. Miyakawa.** 1976. e antigen and anti-e in the serum of asymptomatic carrier mothers as indicators of positive and negative transmission of hepatitis B virus to their infants. N. Engl. J. Med. **294:**746–749.
17. **Orito, E., et al.** 2001. Geographic distribution of hepatitis B virus (HBV) genotype in patients with chronic HBV infection in Japan. Hepatology **34:** 590–594.
18. **Osiowy, C., E. Giles, Y. Tanaka, M. Mizokami, and G. Y. Minuk.** 2006. Molecular evolution of hepatitis B virus over 25 years. J. Virol. **80:**10307–10314.
19. **Pybus, O. G., A. J. Drummond, T. Nakano, B. H. Robertson, and A. Rambaut.** 2003. The epidemiology and iatrogenic transmission of hepatitis C virus in Egypt: a Bayesian coalescent approach. Mol. Biol. Evol. **20:**381–387.
20. **Quarleri, J., et al.** 2007. Hepatitis B virus genotype distribution and its lamivudine-resistant mutants in HIV-coinfected patients with chronic and occult hepatitis B. AIDS Res. Hum. Retroviruses **23:**525–531.
21. **Rambout, A., and A. J. Drummond.** 2007. Tracer v1.4. Institute of Evolutionary Biology, University of Edinburgh, Edinburgh, Scotland. http://tree.bio.ed.ac.uk.
22. **Schaefer, S.** 2007. Hepatitis B virus taxonomy and hepatitis B virus genotypes. World J. Gastroenterol. **13:**14–21.
23. **Shafer, R.** 2010, posting date. Stanford drug resistance database. http://hivdb.stanford.edu/.
24. **Sheldon, J., et al.** 2005. Selection of hepatitis B virus polymerase mutations in HIV-coinfected patients treated with tenofovir. Antivir. Ther. **10:**727–734.
25. **Shiraki, K.** 2000. Perinatal transmission of hepatitis B virus and its prevention. J. Gastroenterol. Hepatol. **15**(Suppl.)**:**E11–E15.
26. **Soriano, V., et al.** 2010. Predictors of hepatitis B virus genotype and viraemia in HIV-infected patients with chronic hepatitis B in Europe. J. Antimicrob. Chemother. **65:**548–555.
27. **Sugauchi, F., et al.** 2001. A novel variant genotype C of hepatitis B virus identified in isolates from Australian Aborigines: complete genome sequence and phylogenetic relatedness. J. Gen. Virol. **82:**883–892.
28. **Suzuki, Y., et al.** 2005. Persistence of acute infection with hepatitis B virus genotype A and treatment in Japan. J. Med. Virol. **76:**33–39.
29. **Swafford, D.** 2003. PAUP. Phylogenetic analysis using parsimony (and other methods), version 4. Sinouer Associates, Sunderland, MA.
30. **Takeda, Y., et al.** 2006. Difference of HBV genotype distribution between acute hepatitis and chronic hepatitis in Japan. Infection **34:**201–207.
31. **Tanaka, J., et al.** 2004. Sex- and age-specific carriers of hepatitis B and C viruses in Japan estimated by the prevalence in the 3,485,648 first-time blood donors during 1995-2000. Intervirology **47:**32–40.
32. **Tenney, D. J., et al.** 2004. Clinical emergence of entecavir-resistant hepatitis B virus requires additional substitutions in virus already resistant to lamivudine. Antimicrob. Agents Chemother. **48:**3498–3507.
33. **Trimoulet, P., et al.** 2007. Hepatitis B virus genotypes: a retrospective survey in southwestern France, 1999-2004. Gastroenterol. Clin. Biol. **31:**1088–1094.
34. **Westland, C. E., et al.** 2003. Week 48 resistance surveillance in two phase 3 clinical studies of adefovir dipivoxil for chronic hepatitis B. Hepatology **38:**96–103.
35. **Yang, H., et al.** 2002. Resistance surveillance in chronic hepatitis B patients treated with adefovir dipivoxil for up to 60 weeks. Hepatology **36:**464–473.
36. **Yotsuyanagi, H., et al.** 2005. Distinct geographic distributions of hepatitis B virus genotypes in patients with acute infection in Japan. J. Med. Virol. **77:**39–46.

PLOS ONE

The Carboxyl-Terminus of Human Immunodeficiency Virus Type 2 Circulating Recombinant form 01_AB Capsid Protein Affects Sensitivity to Human TRIM5α

Tadashi Miyamoto, Emi E. Nakayama, Masaru Yokoyama, Shiro Ibe, Shunpei Takehara, Ken Kono, Yoshiyuki Yokomaku, Massimo Pizzato, Jeremy Luban, Wataru Sugiura, Hironori Sato, Tatsuo Shioda

Published: October 19, 2012 • DOI: 10.1371/journal.pone.0047757

Abstract

Human immunodeficiency virus (HIV) type 2 shows limited geographical distribution compared with HIV type 1. Although 8 genetic groups of HIV type 2 (HIV-2) have been described, recombinant viruses between these groups are rarely observed. Recently, three HIV-2 patients in Japan were described with rapidly progressive, acquired immunodeficiency. These patients were infected with an A/B inter-group recombinant designated CRF01_AB. Here, we characterize the capsid protein (CA) encoded by the viruses from these patients. HIV-2 CRF01_AB CA showed unique amino acid sequence almost equally distinct from group A and group B viruses. Notably, HIV-2 CRF01_AB CA showed potent resistance to human TRIM5α. In addition to the previously identified amino acid position 119 in the N-terminal domain of CA, we found that HIV-2 CRF01_AB-specific amino acid substitutions in the C-terminal domain also were necessary for resistance to human TRIM5α. These results indicate that retroviruses can evade TRIM5α by substitution at residues within the C-terminal domain of CA.

Figures

Citation: Miyamoto T, Nakayama EE, Yokoyama M, Ibe S, Takehara S, et al. (2012) The Carboxyl-Terminus of Human Immunodeficiency Virus Type 2 Circulating Recombinant form 01_AB Capsid Protein Affects Sensitivity to Human TRIM5α. PLoS ONE 7(10): e47757. doi:10.1371/journal.pone.0047757

Editor: Vladimir Brusic, Dana-Farber Cancer Institute, United States of America

Received: July 31, 2012; **Accepted:** September 20, 2012; **Published:** October 19, 2012

Funding: This work was supported by grants from the Health Science Foundation; the Ministry of Education, Culture, Sports, Science, and Technology, Japan (23590541 to EEN, 23390111 to TS), the Ministry of Health, Labour, and Welfare, Japan (H22-AIDS-003 to HS), Swiss National Fund grant 3100A0-128655 to JL, and NIH grant RO1AI59159 to JL. The funders had no role in study design, data collection and analysis, decision to publish, or preparation of the manuscript.

Competing interests: The authors have declared that no competing interests exist.

Introduction

Human immunodeficiency virus type 2 (HIV-2) has been detected primarily in West Africa, in contrast to the global distribution of the type 1 epidemic virus (HIV-1). Based on molecular evidence, HIV-2 and HIV-1 are presumed to derive from simian immunodeficiency viruses that originated in sooty mangabey (SIVsm) and chimpanzee (SIVcpz), respectively, as a result of zoonotic transfer between non-human primates and human. The HIV-1 and HIV-2 bear a considerable degree of homology in both gene organization and RNA sequence (30%–60%) [1]–[4]. It is generally believed that HIV-2 is less pathogenic than HIV-1. However, certain HIV-2 patients with high plasma HIV-2 loads develop acquired immune deficiency syndrome (AIDS) as rapidly as HIV-1 patients do [4]. To date, eight HIV-2 groups have been distinguished on the basis of phylogenetic (sequence) analysis; each group is presumed to have originated from an independent zoonotic event [5].

TRIM5α was identified as a factor that restricts HIV-1 infection in rhesus monkey (Rh) cells [6]. TRIM5α is thought to degrade the core of the incoming virus [7], [8]. TRIM5 proteins are members of the tripartite motif family containing RING, B-box, and coiled-coil domains. The alpha isoform of TRIM5 has an additional C-terminal PRYSPRY (B30.2) domain [9]. In cynomolgus monkey (CM), TRIM5α also has been demonstrated to restrict HIV-1 infection [6], [10]. In contrast, the human TRIM5α exhibits minimal restriction of HIV-1 infection [11]–[14], but shows moderate levels of restriction for HIV-2 [15].

Capsid (CA) proteins are components of the viral core; the CAs of HIV-1 and HIV-2 have similar primary and three dimensional structures [16]. CA is composed of a surface-exposed N-terminal domain (NTD) and a C-terminal domain (CTD) that is required for oligomerization [17]. We previously identified a single amino acid of the HIV-2 capsid that determines the susceptibility of HIV-2 to CM TRIM5α. Viruses that encoded CAs with either alanine or glutamine at amino acid residue 119 (which corresponded to the 120th amino acid of the CA of the GH123 viral strain) could grow in cells harboring the CM TRIM5α. In contrast, HIV-2 encoding CA with proline at the same position showed restricted growth in cells harboring the CM TRIM5α. Similar results, although to a lesser extent, were observed when the human TRIM5α was used [15]. Furthermore, an analysis of HIV-2 CA variation in a West African Caio cohort demonstrated that the presence of proline at CA positions 119, 159, and 178 was more frequent in individuals with lower viral loads (VLs); the presence of non-proline residues at all 3 residues was more frequent in individuals with high VLs. The *in vitro* replication levels of viruses bearing changes at the 3 positions suggested that these 3 residues influence virus replication by altering susceptibility to TRIM5α [18]. These results also suggested that TRIM5α controls virus replication in HIV-2-infected individuals.

Recently, five HIV-2-seropositive cases were identified in Japan. Three isolates (NMC307, NMC716, and NMC842) were recovered from these patients and were shown by full-length genomic analysis to represent a recombinant (designated HIV-2 CRF01_AB) of group A and B strains [19]. Although more than 75% of patients with HIV-2 have asymptomatic prognoses throughout their lifetimes [1], [20], all 3 of the CRF01_AB patients were found to be at an advanced stage of AIDS with low CD4+ cell counts and high HIV-2 VLs [19]. All 3 patients were under 40 years of age when first diagnosed as HIV-2 positive [19]. Assessment of risk factors suggested that all three were infected via heterosexual contacts; no personal connection was confirmed among any of these cases [19]. In the present study, we characterized the HIV-2 CRF01_AB CA obtained from these patients and found several unique properties of HIV-2 CRF01_AB, including potent resistance to human TRIM5α-mediated restriction.

Results

HIV-2 CRF01_AB Strains Show Unique CA Sequences

Fig. 1 shows an alignment of the deduced amino acid sequences of the CAs of HIV-2 group A (ROD, UC12, GH123, and UC2), HIV-2 group B (UC14, D205, and UC1), SIVs (SIVmac239 and SIVsm PBJ14), and HIV-2 CRF01_AB (NMC307, NMC716, NMC842, and 7312A). As we reported previously [15], [18], the 119th amino acid position is a proline, glutamine, or alanine in the CAs of HIV-2 group A, HIV-2 group B, and SIVs. However, the CAs of the HIV-2 CRF01_AB strains uniquely possess a glycine at this position. Based on the genomic structure of HIV-2 CRF01_AB, A/B recombinant breakpoints within this isolate are located near or within the *env* gene, such that HIV-2 CRF01_AB can be considered to consist of a group B backbone that incorporates group A *env* fragments [19]. These presumed breakpoints could be taken to suggest that CRF01_AB CA should be encoded as a B-like sequence. However, phylogenetic analysis of these CA sequences (Fig. 2) reveals that the deduced HIV-2 CRF01_AB CA proteins constitute a distinct cluster, with the dendrogram exhibiting a long branch length compared to the CAs of HIV-2 group A, HIV-2 group B, and SIV.

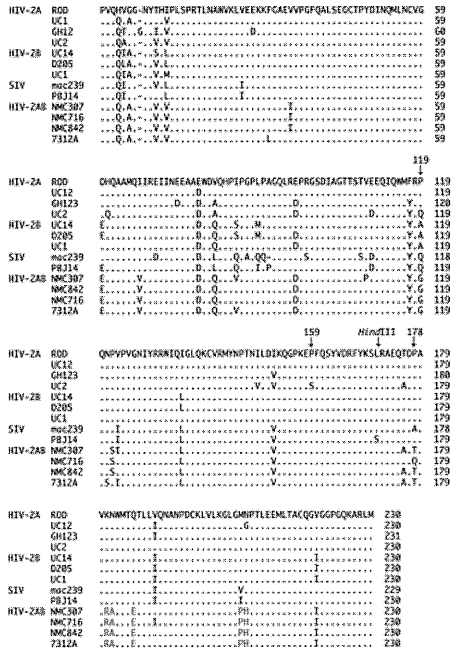

Figure 1. Alignments of amino acid sequences of CA proteins encoded by selected HIV-2 isolates and SIV from the Los Alamos databases.
Dots denote amino acid identity with the ROD CA; dashes denote gaps introduced to optimize alignment. HIV-2 CRF01_AB-specific amino acid residues are in red. Arrows indicate key residues at 119, 159, and 178, and the position (in the corresponding DNA sequence) of the *Hind*III restriction site used in the constructs. HIV-2A, HIV-2B, and HIV-2AB denote HIV-2 group A, HIV-2 group B, and HIV-2 CRF01_AB, respectively.
doi:10.1371/journal.pone.0047757.g001

HIV-2 CRF01_AB CA is Highly Resistant to Human TRIM5α

In a previous study, we reported that the amino acid at residue 119 of the HIV-2 CA affects susceptibility to the restriction of virus replication by CM and human TRIM5α [15], such that HIV-2 encoding CA(Pro119) was sensitive to CM and human TRIM5α, while HIV-2 encoding CA(Gln119) or CA(Ala119) was resistant [15]. We also reported that mutation of HIV-2 strain GH123 to encode glycine at the corresponding position (GH123/G) rendered GH123 resistant to CM TRIM5α [21]. To further test the role of the CA protein in TRIM5α resistance, we generated recombinant versions of the GH123 virus (716 or 842) in which the CA-encoding segment of *gag* was replaced with that of the A/B recombinants NMC716 or NMC842 (respectively). We used a recombinant Sendai virus (SeV) system to express CM, Rh, and human TRIM5α and CM TRIM5α lacking the PRYSPRY domain as a negative control (Fig. S1). In the presence of CM TRIM5α, infection by the parental GH123 virus was restricted, but infection by GH123/G was resistant to CM TRIM5α-mediated restriction (Fig. 3A). Infection by 716 or 842 was resistant to CM TRIM5α (Fig. 3B). In contrast, infection by any of the 4 variants (GH123, GH123/G, 716, and 842) was completely restricted by Rh TRIM5α (Fig. 3A, B). These results for cells producing CM or Rh TRIM5α are consistent with our previous findings [22]. In cells producing human TRIM5α, the replication of parental GH123 and of the GH123/G mutant were partially restricted (Fig. 3A), while 716 and 842 replicated as efficiently as in negative control cells that did not produce a functional TRIM5α (Fig. 3B). The mean ratios of the p25 levels at 6 days after infection in the cells producing human TRIM5α to those in the negative control cells were 0.14 for GH123, 0.30 for GH123/G, but 0.81 for 716 and 1.02 for 842 in three independent experiments. The ratio of GH123/G was significantly higher than that of GH123 ($P = 0.0086$, t test) but lower than those of 716 ($P = 0.0059$, t test) and 842 ($P = 0.0030$, t test). Similar results were obtained when we calculated the mean ratios of the p25 levels at 3 days after infection (data not shown). These data indicate that the CA sequences of the CRF01_AB strains conferred higher potential to escape from human TRIM5α than those of GH123/G.

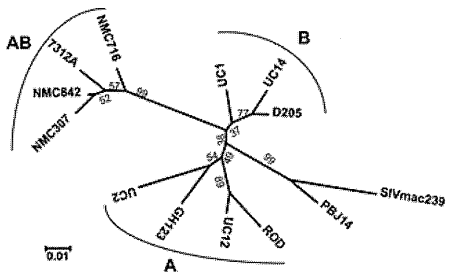

Figure 2. Phylogenetic tree of HIV-2 isolates and SIV.
This phylogenetic tree was constructed by the neighbor-joining method. Bootstrap probabilities (%), as calculated by 1000 iterations, are shown at the major tree nodes. Scale bar represents 0.01 amino acid substitutions per site. A, B, and AB denote HIV-2 group A, HIV-2 group B, and HIV-2 CRF01_AB, respectively.
doi:10.1371/journal.pone.0047757.g002

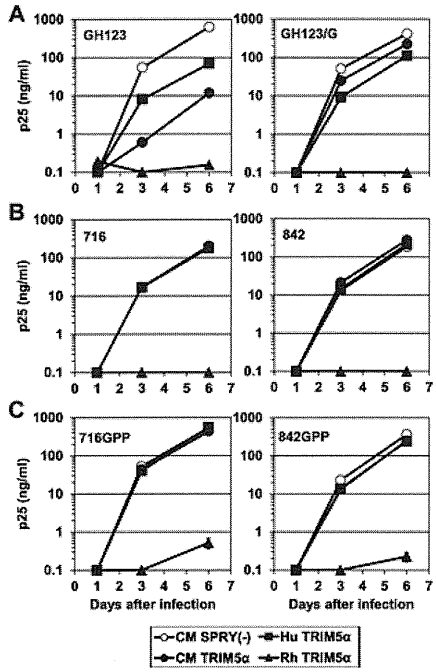

Figure 3. Growth of HIV-2 strain GH123 and variants thereof in the presence of TRIM5α.
(A), (B), (C) Virus levels were measured by ELISA detection of p25 (CA) levels in supernatants. CEM-SS cells were infected with recombinant SeV encoding rhesus (Rh: black triangles); cynomolgus monkey (CM: black circles); human (Hu: black squares); or CM SPRY(-) (white circles) TRIM5α. CM SPRY (-) has a dominant negative effect on the anti-viral activity of TRIM5α and serves as a negative control. Nine hours after infection, cells were superinfected with GH123, GH123/G, 716, 842, 716GPP, or 842GPP. Error bars show actual fluctuations between levels of p25 (CA) in duplicate samples from one of three independent experiments.
doi:10.1371/journal.pone.0047757.g003

Viral Sensitivity to Human TRIM5α-mediated Restriction in a Single Round Infection Assay

TRIM5α restricts viral infection at a post-entry step [6], [23], [24]. To focus on early steps of virus replication, we performed a single-round infection assay, in which infection is detected as fluorescence generated by production of the green fluorescent protein (GFP). To construct mutant viruses encoding GFP, the fragment of GH123, 842, or GH123/G that encoded the matrix (MA) and CA proteins was transferred to the *env*-disrupted HIV-2 genomic clone pROD-env(-)-GFP, which directs the production of GFP after infection [25]. Vesicular stomatitis virus glycoprotein (VSV-G) pseudotyped wild-type and mutant HIV-2 GFP viruses were inoculated into feline CRFK cells producing TRIM5α, and GFP-positive cells were counted 2 days after infection. In this experiment, we used feline cells, since feline cells lack expression of endogenous TRIM5α. In the presence of CM TRIM5α, the numbers of GFP-positive cells were greater in cells infected with GFP-expressing viruses encoding the GH123/G or 842 CAs than in those infected with the GFP-expressing viruses encoding GH123 CA (Fig. 4), confirming that viruses encoding CA(G119) were resistant to CM TRIM5α. Consistent with the results shown in Fig. 3B, the GFP-expressing virus encoding the 842 CA from a patient was more resistant to human TRIM5α-mediated restriction than viruses encoding the CAs from GH123 ($P = 0.0010$, t-test) or GH123/G ($P = 0.0026$, t-test) (Fig. 4).

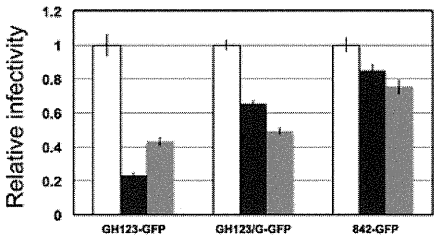

Figure 4. Viral sensitivity to TRIM5α-mediated restriction in a single-round infection assay.
Feline CRFK cells were infected with SeV encoding cynomolgus monkey (CM; black bars), human (grey bars), or CM SPRY(-) (white bars) TRIM5α. CM SPRY (-) has a dominant negative effect on the anti-viral activity of TRIM5α and serves as a negative control. The cells then were superinfected with a green fluorescent protein (GFP)-expressing virus, GH123-GFP, GH123/G-GFP, or 842-GFP containing 500ng of p25 (CA). Two days after infection, the cells were fixed by formaldehyde, and GFP-producing cells were counted by flow cytometry. Numbers of GFP-positive cells in CM SPRY (-)-producing cells are set at one and relative numbers to CM SPRY (-) of GFP-positive cells are shown. Error bars denote standard deviations of triplicate samples from one of three independent experiments.
doi:10.1371/journal.pone.0047757.g004

Viral Growth in TRIM5α Knock-down Cells

We next investigated whether the different resistance to human TRIM5α restriction among recombinant HIV-2 strains still applied in cells producing physiological levels of human TRIM5α protein. For this purpose, we used TRIM5α "knock-down" Jurkat cells (TRIM5α-KD Jurkat) and the corresponding control Jurkat line (Luci-siRNA Jurkat) [26]. It was demonstrated that the level of TRIM5α mRNA in TRIM5α-KD Jurkat is five times lower than that of Luci-siRNA Jurkat by TaqMan quantitative PCR. Three days after infection, GH123 replicated better in TRIM5α-KD Jurkat than in Luci-siRNA Jurkat (Fig. 5A). On the other hand, GH123/G, 716, and 842 yielded comparable titers in both cell lines (Fig. 5B, 5C, and 5D). In this experiment, we found that GH123/G also was resistant to human TRIM5α. Nevertheless, the data presented in Fig. 5 indicated that GH123 was sensitive to human TRIM5α produced at physiologically relevant levels, while 716 and 842

possessed potent resistance against human TRIM5α. Since TRIM5α-KD Jurkat always showed reduced proliferative properties compared to Luci-siRNA Jurkat (data not shown), presumably due to reduced TRIM5α levels [27], the p25 levels of all these viruses in Luci-siRNA Jurkat became higher than those in TRIM5α-KD Jurkat at 10 days after infection (data not shown).

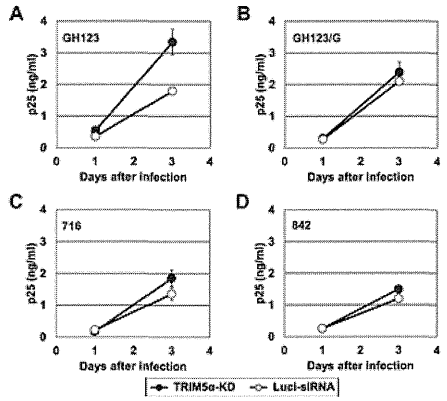

Figure 5. Viral growth in TRIM5α knock-down cells.
(A), (B), (C) and (D) TRIM5α-KD Jurkat ("knock-down") or Luci-siRNA Jurkat (control) cells were infected with derivatives of GH123 virus. Culture supernatants were periodically assayed for levels of virus capsid. Error bars show actual fluctuations of duplicate samples from one of two independent experiments. Black and white bars denote TRIM5α-KD Jurkat and Luci-siRNA Jurkat cells, respectively.
doi:10.1371/journal.pone.0047757.g005

HIV-2 CRF01_AB CA C-terminal Domain-specific Sequence also Affects Viral Sensitivity to Human TRIM5α

We previously reported that the presence of proline at CA positions 119, 159, and 178 is more frequent in individuals with lower VLs [18]. Viral isolates NMC307, NMC716, and NMC842 all encoded CAs with proline at the 159th position (Fig. 1). However, the 178th amino acid residue was encoded as a threonine (NMC307 and NMC842) or as a glutamic acid (NMC716) in these isolates (Fig. 1). To test whether a single residue at amino acid 178 of HIV-2 CRF01_AB CA affects the sensitivity to human TRIM5α, we generated recombinant 716 or 842 viruses (designated 716GPP or 842GPP, respectively) that encoded CA (Pro178) proteins. As shown in Fig. 3C, 716GPP and 842GPP escaped from human TRIM5α restriction as efficiently as 716 and 842 did. These data suggest the existence of viral determinants for human TRIM5α-resistance other than the previously identified 119th and 178th amino acid positions of CA.

To search for the viral determinants of human TRIM5α resistance other than the 119th and 178th amino acid positions of HIV-2 CA, we constructed a chimeric virus 842Hind by replacing the segment of the 842 genome that encodes CA C-terminal residues 170 to 231 with the corresponding region of GH123 (Fig. 6A). When tested in cells that produced human TRIM5α, 842 was strongly resistant to human TRIM5α as expected (Fig. 6B). However, the 842Hind construct, which encoded the NMC842 CA with the GH123 CA C-terminal short region, lost this resistance to human TRIM5α (Fig. 6C). The mean ratios of the p25 levels at 6 days after infection in the cells producing human TRIM5α to those in the negative control cells were 0.73 for 842 and 0.16 for 842Hind in three independent experiments. The ratio of 842Hind was significantly lower than that of 842 ($P = 0.0003$, t test). Similar results were obtained when we calculated the mean ratios of the p25 levels at 3 days after infection (data not shown). These results suggest that one or more of the HIV-2 CRF01_AB-specific amino acid residues within the CA C-terminal short region (Fig. 1, shown in red) also are necessary to fully evade human TRIM5α.

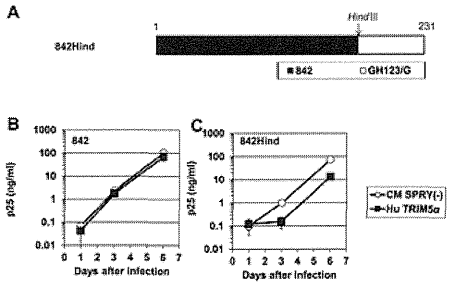

Figure 6. HIV-2 CRF01_AB CA C-terminal domain-specific sequence also affects viral sensitivity to human TRIM5α.
(A) Schematic representation of chimeric viral CAs. Black and white bars show 842 and GH123/G CA peptide sequences, respectively. An arrow denotes the position (in the corresponding DNA sequence) of the *Hind*III restriction site used in the construct. (B and C) CEM-SS cells were infected with recombinant SeV encoding human (Hu: black squares) or CM SPRY(-) (white circles) TRIM5α. Nine hours after infection, cells were superinfected with 842 (B) and 842Hind (C). Culture supernatants were assayed for levels of p25 (CA). Error bars show actual fluctuations between levels of p25 (CA) in duplicate samples from one of three independent experiments.
doi:10.1371/journal.pone.0047757.g006

Molecular Dynamics of N-terminal Domain (NTD) of HIV-2 CRF01_AB CA

Residue 120 of the GH123 CA, which corresponds to residue 119 of the CRF01_AB CA, is located in the loop between α-helices 6 and 7 (L6/7) of CA NTD. Our previous molecular dynamics simulation study of HIV-2 CA NTD revealed that mutations at this position affected conformation of the neighboring loop between α-helices 4 and 5 (L4/5), and TRIM5α-sensitive viruses were predicted to share a common L4/5 conformation. In addition, the shared L4/5 structures of the sensitive viruses were associated with a decreased probability of hydrogen bond formation between GH123 CA's Asp97 (in L4/5) and Arg119 (corresponding to residue 118 in HIV-2 CRF01_AB CA; in L6/7) [21]. TRIM5α-resistant viruses exhibited a variable L4/5 conformation and a higher probability of hydrogen bond formation between L4/5 and L6/7 [21]. As noted above, HIV-2 CRF01_AB strains have a unique Gly119 (Fig. 1), which we had not previously modeled by molecular dynamics simulation. Therefore, three-dimensional (3-D) models of HIV-2 GH123/G and NMC842 CA NTD were constructed using homology modeling based on the crystal structures of the HIV-2 CA NTD, and the models were subjected to molecular dynamics simulation to compare the results with those derived from previously constructed 3-D structural models of TRIM5α-sensitive GH123 and TRIM5α-resistant GH123/Q and GH123/A [21]. GH123/Q and GH123/A encode CA (Gln120) and CA (Ala120), respectively [15]. Contrary to our expectation, the predicted L4/5 conformations of the NTDs of the NMC842 CA and GH123/G CA differed from those of TRIM5α-resistant GH123/Q and GH123/A, better resembling that predicted for the CA NTD encoded by TRIM5α-sensitive GH123 (Fig. 7). Indeed, the calculated

probability of hydrogen bond formation between L4/5 and L6/7 was even lower for the CAs of GH123/G (20.80%) and NMC842 (30.58%) compared to that of GH123 (44.6%). These results suggest that Gly119 endows the CRF01_AB CA NTD with unique structural properties.

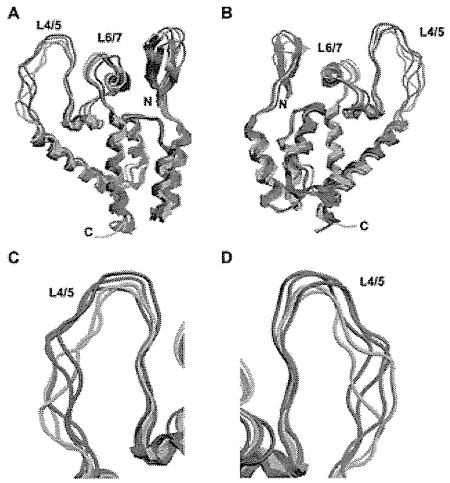

Figure 7. Structural models of the HIV-2 capsid N-terminal domain.
Models were constructed by homology modeling and molecular dynamics simulations with the high-resolution X-ray crystal structure of the HIV-2 capsid N-terminal domain (CA NTD) (PDB code: 2WLV [16]) as the starting structure. Averaged conformations of the overall structure of the CA NTD (from the amino acid position 1 to 150) during 5–20 nanoseconds of MD simulations (A and B) and a close-up view around the L4/5 loop (C and D) are indicated. N and C indicate the amino termini and carboxyl termini, respectively. Models are color coded as follows: red, 842; blue, GH123/G; green, CM TRIM5α-resistant viruses (GH123/Q and GH123/A); and purple, CM TRIM5α-sensitive virus (GH123/P).
doi:10.1371/journal.pone.0047757.g007

Steric Locations of HIV-2 CRF01_AB-specific Amino Acid Substitutions

As noted above, HIV-2 CRF01_AB strains have several specific amino acid substitutions at the C-terminal domain (CTD) of CA (Fig. 1, shown in red); these substitutions were necessary for the potent resistance of these isolates against human TRIM5α (Fig. 6). Previously, we suggested that magnitudes of the computationally calculated binding energies of the CA CTD dimer models tend to be significantly greater in the TRIM5α-less-sensitive HIV-2s in West Africa [18]. To examine if the HIV-2 CRF01_AB-specific amino acid substitutions in CA CTD could influence the CTD-CTD dimer stability, we constructed the CA CTD dimer model of HIV-2 CRF01_AB NMC842 by homology modeling and analyzed steric locations of the specific substitutions and binding energies of the CTD dimer model. In the CA CTD dimer model of NMC842, HIV-2 CRF01_AB-specific amino acid substitutions are located in helix 9 and in the loop between helices 10 and 11, and all appeared to be situated near but distinct from the CTD-CTD dimer interface (Fig. 8A). The predicted binding energy of the CTD-CTD dimer model of the NMC842 isolate (79.6 kcal/mole) was similar to that reported in TRIM5α sensitive viruses [18]. The results may imply that the HIV-2 CRF01_AB-specific amino acid substitutions in CTD do not necessarily influence the CTD-CTD dimer stability of the TRIM5α sensitive virus.

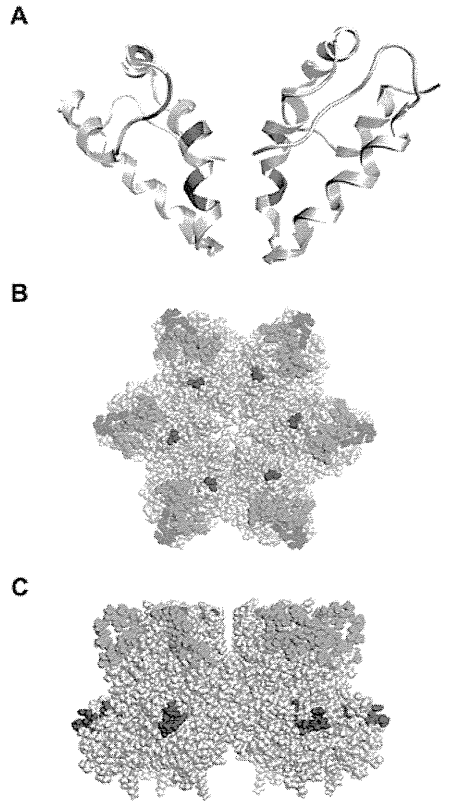

Figure 8. Structural models of the HIV-2 capsid C-terminal domain in dimeric form (A) and the HIV-2 GH123 capsid hexamer (B and C).
(A) The C-terminal domain dimer model (from the amino acid position 150 to 219) of HIV-2 capsid (CA) is based on the viral sequence of NMC842. HIV-2

CRF01_AB-specific amino acid substitutions are shown in red. (B and C) The space-filling model of CA hexamer from the top (B) and side (C) is shown. Positions of HIV-2 CRF01_AB-specific amino acid substitutions are shown in red. L4/5 and 120P are shown in green and blue, respectively.
doi:10.1371/journal.pone.0047757.g008

To further obtain structural insights into the roles of these CRF01_AB-specific mutations, we analyzed their steric locations in the CA hexamer. In the hexamer model of GH123 CA that we previously constructed based on the HIV-1 CA hexamer [28], HIV-2 CRF01_AB-specific amino acid substitutions in CTD form clusters and are located at the outermost part of the hexamer (Fig. 8B and C). Notably, these substitutions exist directly under the L4/5 of neighboring CA (Fig. 8C), and most of them are clearly visible from right above (Fig. 8B). These results raise a possibility that HIV-2 CRF01_AB-specific amino acid substitutions in CA CTD may be exposed to and accessible from the outside of the viral core.

Discussion

In the present study, we have shown that the CA of HIV-2 CRF01_AB isolates have a unique feature distinct from that of other HIV-2 strains; CRF01_AB-specific sequences conferred strong resistance to human TRIM5α. In addition to the previously identified role of amino acid 119 of the CA NTD, CRF01_AB-specific amino acid substitutions in the CA CTD also were necessary for strong resistance to human TRIM5α. These amino acid substitutions in CA CTD may be exposed to and accessible from the outside of the viral core.

Retroviral CA is known to form hexamers [29]. The CTD domain of retroviral capsid protein participates in CA dimerization, where intermolecular CTD-CTD interactions are mediated by symmetric, parallel dimerization of helix 9 from the CTD domains of adjacent hexamers [30]. This dimerization process is prerequisite for assemblies of multiple hexamers [29]. Previously, we found that the computationally calculated binding energies of the CA CTD dimer models could have positive relations with the TRIM5α susceptibilities of HIV-2s in West Africa [18]. We therefore calculated here the binding energy of the CTD-CTD dimer model of the NMC842 using computational method. However, the predicted binding energy of the CTD-CTD dimer of the NMC842 isolate was rather similar to that reported in TRIM5α sensitive viruses [18]. Therefore, previously undescribed mechanisms may be involved in the TRIM5α resistance of the HIV-2 CRF01_AB.

A possible mechanism for the findings may be that the CRF01_AB-specific substitutions influence directly or indirectly the structural properties of an interaction surface for the TRIM5α mediated inhibition. In this regard, we previously suggested with SIV that not only the NTD but also the CTD might constitute an intermolecular interaction surface [31]. Similarly, HIV-2 may have such interaction surface in CTD domain, and the surface may be used for the TRIM5α-mediated inhibition. Results on the steric locations of the CRF01_AB-specific substitutions in the hexamer model support this possibility (Fig. 7B and C). A preliminary modeling study of the assemblies of the CA hexamers also have supported this possibility: the NTDs are apart from each other among the hexamers, which allows to form accessible surface on the CTDs (data not shown), as suggested with Rous sarcoma virus CA [32]. Therefore, it would be interesting to examine whether HIV-2 CRF01_AB-specific amino acid substitutions in CTD could constitute a binding cleft for the TRIM5α itself or others involved in TRIM5α medicated inhibition in the assemblies of multiple CA hexamers in the viral core. Further study is necessary to address this issue.

Previously, we showed that the amino acid replacements at CA residue 119 affected the conformation of the neighboring L4/5, and that TRIM5α-sensitive viruses had a shared L4/5 conformation that was associated with a decreased probability of hydrogen bonding between L4/5 and L6/7 [21]. Although GH123/G and 842 showed resistance to TRIM5α, the calculated probability of hydrogen bond formation between L4/5 and L6/7 was lower than that calculated for the CAs of other TRIM5α-resistant viruses, including that from GH123/Q (55.15%) and GH123/A (64.47%) [21]. The conformations of L4/5 in the CAs of GH123/G and 842 also were similar to those of TRIM5α-sensitive viruses, and were distinct from those of the CAs of TRIM5α-resistant viruses. These characteristics of GH123/G and 842 were similar to those of GH123/E and GH123/D, mutant GH123 clones encoding glutamic acid and aspartic acid (respectively) at the residue corresponding to position 119 of HIV-2 CRF01_AB strains [21]. Although glutamic acid and aspartic acid have not been observed at this CA residue in HIV-2 isolated clinically, both GH123/E and GH123/D showed resistance against CM TRIM5α. In contrast to the CAs of GH123/Q and GH123/A, the CAs of both GH123/E and GH123/D show reduced likelihoods of hydrogen bond formation between the L4/5 and L6/7, and the L4/5 conformations were predicted to be similar to those of the CAs of TRIM5α-sensitive viruses. Therefore, our present results extend our previous observations, and additionally imply that the Gly119 of HIV-2 CRF01_AB CA prevents binding by TRIM5α, probably due to the small size of the glycine side chain. It is possible that the shared conformation of L4/5 might have some advantages in utilizing certain cellular factor(s) that bind CA. Our structural data suggests that HIV-2 CRF01_AB strains are highly adapted, since these strains have acquired potent resistance against TRIM5α without losing the shared L4/5 conformation.

In the case of GH123/E, disruption of the hydrogen bond between L4/5 and L6/7 by substitution of alanine for aspartic acid at position 97 (D97A) did not alter the resistant phenotype of GH123/E [21], while the same substitution almost completely abolished the replicative ability of GH123/G (data not shown). This result further demonstrates the unique status of GH123/G, since D97A substitution did not cause such a drastic reduction of replicative ability in GH123, GH123/Q, and GH123/A [21]. The basis for the difference between GH123/G and other variants is unclear; further mutational studies will be necessary to elucidate detailed interactions between L4/5 and L6/7, and to define the contribution of these sequences to viral replication and TRIM5α sensitivity.

In the Los Alamos databases, almost all SIV isolates encode glutamine at the position corresponding to residue 119 of the HIV-2 CRF01_AB CA. It is likely that the sequential mutation from glutamine (coded as CAA or CAG) to proline (CCA or CCG; underlines denote single nucleotide changes) and then to alanine (GCA, GCG) occurred after transmission of the monkey virus to the human population. The nature of the genetic code suggests that the Gly119-encoding virus (GGA or GGG codon) derived from the Ala119-encoding virus, implying that the viruses with glycine are highly adapted, as also discussed above. A single HIV-2 strain encoding glycine at the 119th CA residue was found in the Los Alamos databases; this strain (7312A) was isolated from a symptomatic 32-years-old man [33], and also was a recombinant between groups A and B (Fig. 1 and 2). This recombinant virus exhibits a genomic organization similar to that of NMC307, NMC716, and NMC842. At present, we do not know whether the emergence of glycine at the 119th position of CA is unique to HIV-2 CRF01_AB. It will be critical to assess the emergence of Gly119 viruses within HIV-2 groups A and B.

It is generally believed that HIV-2 is less pathogenic than HIV-1, and the number of HIV-2 cases is now gradually decreasing in West Africa. However, NMC307, NMC716, and NMC842 were recovered from patients at an advanced stage of AIDS with low CD4+ cell counts and high HIV-2 VLs [19]. It is possible that these HIV-2 CRF01_AB strains are highly pathogenic, unlike other HIV-2 strains. Careful epidemiological and virological studies are necessary to test this hypothesis. In the present study, we found that HIV-2 CRF01_AB CA confers strong resistance to human TRIM5α. In the Caio HIV-2 cohort in West Africa, non-proline residues at position 119 were significantly associated with elevated plasma HIV-2 load [18]. Therefore, resistance to TRIM5α may at least partially explain why these 3 patients in Japan developed AIDS so rapidly, although the possible effects of mutations in regions (e.g., *env*, *vif*, *nef* and the long terminal repeats) other than those that encode CA cannot be fully excluded at present. Our results also suggest that resistance to TRIM5α might be a new marker for the pathogenic potential of HIV-2. The possible emergence of a highly pathogenic HIV-2 strain is an ongoing concern, given that retroviruses can easily evolve to evade host defenses.

Materials and Methods

Phylogenetic Tree Analysis

Multiple sequence alignment was performed using the software CLUSTALW version 2.1. Phylogenetic trees were constructed using the neighbor-joining method. Bootstrap probabilities were calculated by 1000 iterations [34].

Cell Culture

The human 293T [35] and feline CRFK [36] cells were maintained in Dulbecco's Modified Eagle medium. The human T-cell line CEM-SS [37] was maintained in RPMI medium. All media were supplemented with 10% fetal bovine serum and 1% penicillin-streptomycin.

Plasmid Construction

Recombinant HIV-2 GH123 clones containing the entire CA sequence of the isolates NMC716 or NMC842 (716 or 842, respectively) and 716 or 842 with proline substitutions at the 178th position (716GPP or 842GPP, respectively) were generated by PCR-based mutagenesis. The GH123/G virus was described previously [21]. The 0.6-kb *Hind*III-*Xho*I fragment of 842 was replaced with the corresponding fragment of GH123/G, and the resulting plasmid was designated 842Hind. Infectious viruses were prepared by transfection of 293T cells with the resulting proviral DNA clones. Viral titers were determined by measuring P25 (CA) with a RetroTek antigen ELISA kit (ZeptoMetrix, Buffalo, NY).

To construct the wild-type and mutant HIV-2 clones encoding GFP, the 1.6-kb *Kpn*I-*Xho*I fragment (which encodes the MA, CA and p6) of GH123, 842, or GH123/G, was transferred to pROD-env(-)-GFP [25], a clone in which the *env* gene is disrupted, and the GFP gene was inserted into the *nef* region. Infectious viruses were prepared by transfection of 293T cells with proviral DNA clones together with the pMD2G plasmid encoding VSV-G. Viral titers were determined as above.

Construction of recombinant SeV encoding C-terminally HA-tagged CM TRIM5α (CM-TRIM5α-SeV), Rh TRIM5α (Rh-TRIM5α-SeV), human TRIM5α (Hu-TRIM5α-SeV), and CM TRIM5α lacking the PRYSPRY domain (CM-SPRY(-)-SeV) were described previously [10], [15], [22].

Viral Infection

CEM-SS cells (1×10^6) were infected with SeVs encoding the respective TRIM5α proteins at a multiplicity of infection of 10 plaque-forming units per cell and incubated at 37°C for 9 h. Aliquots of 1×10^5 cells were then superinfected with GH123, GH123/G, 716, 716GPP, 842, 842GPP, or 842Hind virus. Each superinfection used a titer of virus corresponding to 20 ng of p25 (CA). Experiment was performed three separate times with duplicate samples. For viral infection of cells producing physiological levels of TRIM5α, TRIM5α knock-down Jurkat cells (TRIM5α-KD Jurkat) and control cells (Luci-siRNA Jurkat) were infected with GH123, GH123/G, 716, or 842 virus. Each infection used a titer of virus corresponding to 100 ng of p25. The culture supernatants were collected periodically, and the level of p25 (CA) was measured as described above. Experiment was performed two separate times with duplicate samples.

Western Blot

CEM-SS cells (1×10^6) infected with recombinant SeVs expressing HA-tagged TRIM5α proteins were lysed in lysis buffer (50 mM Tris-HCl, pH 7.5, 150 mM NaCl, 1% Nonidet P40, 0.5% sodium deoxycholate). TRIM5α proteins in the lysates were subjected to sodium dodecyl sulfate-polyacrylamide gel electrophoresis. Proteins in the gel were then electronically transferred onto a membrane (Immobilon; Millipore, Billerica, MA). Blots were blocked and probed with anti-HA high-affinity rat monoclonal antibody (Roche, Indianapolis, IN) overnight at 4°C. Blots were then incubated with peroxidase-conjugated anti-rat IgG (American Qualex, San Clemente, CA), and bound antibodies were visualized with a Chemilumi-One chemiluminescent kit (Nacalai Tesque, Kyoto, Japan).

Single-round Infection Assay

SeV-infected CRFK cells (4×10^4) were infected with a titer of pROD-env(-)-GFP derivative virus corresponding to 500 ng of p25 (CA). Two days after infection, the cells were fixed by formaldehyde, and GFP-producing cells were counted by flow cytometry. Experiment was performed three separate times with triplicate samples.

Molecular Modeling and MD Simulation

We used molecular dynamic (MD) simulations [38] to analyze the structural dynamics of the HIV-2 CA NTDs. First, initial CA structures for MD simulation were constructed by homology modeling [39] using the Molecular Operating Environment, MOE (Chemical Computing Group Inc., Montreal, Canada) as described previously [15], [40]. We used the high-resolution crystal structure of the HIV-2 CA NTD at a resolution of 1.25Å (PDB code: 2WLV) [16] as the modeling template. Structural dynamics of these HIV-2 CA models in an aqueous environment were analyzed using MD simulations with the SANDER module in the AMBER 9 program package [41] and the AMBER99SB force field with the TIP3P water model [42]. Bond lengths involving hydrogen were constrained with SHAKE [43] and the time step for all MD simulations was set to 2 fs. After heating calculations for 20 ps to 310 K using the NVT ensemble, the simulations were executed using the NPT ensemble at 1 atm and 310 K for 20 ns. Hydration analyses were performed using the ptraj module in AMBER. A maximum cut-off angle of 120.0° and cut-off length of 3.5 Å were used in hydrogen bond definitions.

For the CTD dimer model of HIV-2 CRF01_AB NMC842, a crystal structure of the HIV-1 CA protein was used as the template for the modeling; the dimer of CA C-terminal domain at a resolution of 1.70 Å (PDB code: 1A8O) [17]. The amino acid sequence identity of HIV-1 (1A8O) and HIV-2 CA (NMC842 in this study) is about 76%. The sequence similarity is sufficient to construct a structural model with an r.m.s. deviation of approximately 1.5 Å for the main chain between the predicted and actual structures [39]. The 3-D structures were optimized thermodynamically by energy minimization using MOE and an AMBER99 force field [44] and further refined the physically unacceptable local structures on the basis of evaluation of unusual dihedral angles, *phi* and *psi*, by the Ramachandran plot using MOE. The binding energies of the CA dimer models, E_{bind}, were calculated as described elsewhere [45], [46], using the formula $E_{bind} = E_{dimer}–2E_{monomer}$, where E_{dimer} is the energy of the CA dimer; $E_{monomer}$ is the energy of the CA monomer.

Conclusions

The CA of HIV-2 CRF01_AB isolates have a unique feature distinct from that of other HIV-2 strains; CRF01_AB-specific sequences conferred strong resistance to human TRIM5α. CRF01_AB-specific amino acid substitutions in the CA CTD were necessary for strong resistance to human TRIM5α.

Supporting Information

Figure_S1.eps

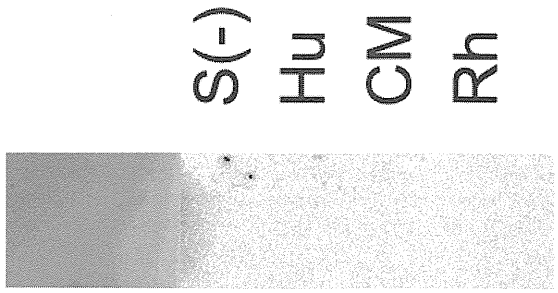

figshare download

Western blot analysis of TRIM5α proteins. HA-tagged TRIM5α proteins in lysate of CEM-SS cells infected with recombinant SeV were visualized by western blotting with an antibody against HA. S(-), Hu, CM, and Rh denote CM SPRY(-), human, cynomolgus monkey, and rhesus TRIM5α, respectively. Molecular weight makers are shown on the left.

Figure S1.
Western blot analysis of TRIM5α proteins. HA-tagged TRIM5α proteins in lysate of CEM-SS cells infected with recombinant SeV were visualized by western blotting with an antibody against HA. S(-), Hu, CM, and Rh denote CM SPRY(-), human, cynomolgus monkey, and rhesus TRIM5α, respectively. Molecular weight makers are shown on the left.
doi:10.1371/journal.pone.0047757.s001
(EPS)

Acknowledgments

We thank Dr. Y. Tian, Dr. S. Nakamura and Dr. T. Yasunaga for helpful discussions, and Ms. S. Bando and Ms. N. Teramoto for assistance.

Author Contributions

Conceived and designed the experiments: TM EEN SI HS TS. Performed the experiments: TM EEN MY ST KK. Analyzed the data: TM EEN MY SI KK JL WS HS TS. Contributed reagents/materials/analysis tools: SI YY MP JL WS. Wrote the paper: TM EEN MY SI JL HS TS.

References

1. Rowland-Jones SL, Whittle HC (2007) Out of Africa: what can we learn from HIV-2 about protective immunity to HIV-1? Nat Immunol 8: 329–331. doi: 10.1038/ni0407-329
View Article • PubMed/NCBI • Google Scholar

2. Gao F, Bailes E, Robertson DL, Chen Y, Rodenburg CM, et al. (1999) Origin of HIV-1 in the chimpanzee Pan troglodytes troglodytes. Nature 397: 436–441. doi: 10.1038/17130
View Article • PubMed/NCBI • Google Scholar

3. Huet T, Cheynier R, Meyerhans A, Roelants G, Wain-Hobson S (1990) Genetic organization of a chimpanzee lentivirus related to HIV-1. Nature 345: 356–359. doi: 10.1038/345356a0
View Article • PubMed/NCBI • Google Scholar

4. Gottlieb GS, Sow PS, Hawes SE, Ndoye I, Redman M, et al. (2002) Equal plasma viral loads predict a similar rate of CD4+ T cell decline in human immunodeficiency virus (HIV) type 1- and HIV-2-infected individuals from Senegal, West Africa. J Infect Dis 185: 905–914. doi: 10.1086/339295
View Article • PubMed/NCBI • Google Scholar

5. Damond F, Worobey M, Campa P, Farfara I, Colin G, et al. (2004) Identification of a highly divergent HIV type 2 and proposal for a change in HIV type 2 classification. AIDS Res Hum Retroviruses 20: 666–672. doi: 10.1089/0889222041217392
View Article • PubMed/NCBI • Google Scholar

6. Stremlau M, Owens CM, Perron MJ, Kiessling M, Autissier P, et al. (2004) The cytoplasmic body component TRIM5alpha restricts HIV-1 infection in Old World monkeys. Nature 427: 848–853. doi: 10.1038/nature02343
View Article • PubMed/NCBI • Google Scholar

7. Sebastian S, Luban J (2005) TRIM5alpha selectively binds a restriction-sensitive retroviral capsid. Retrovirology 2: 40. doi: 10.1186/1742-4690-2-40
View Article • PubMed/NCBI • Google Scholar

8. Stremlau M, Perron M, Lee M, Li Y, Song B, et al. (2006) Specific recognition and accelerated uncoating of retroviral capsids by the TRIM5alpha restriction factor. Proceedings of the National Academy of Sciences of the United States of America 103: 5514–5519. doi: 10.1073/pnas.0509996103
View Article • PubMed/NCBI • Google Scholar

9. Reymond A, Meroni G, Fantozzi A, Merla G, Cairo S, et al. (2001) The tripartite motif family identifies cell compartments. Embo J 20: 2140–2151. doi: 10.1093/emboj/20.9.2140
View Article • PubMed/NCBI • Google Scholar

10. Nakayama EE, Miyoshi H, Nagai Y, Shioda T (2005) A specific region of 37 amino acid residues in the SPRY (B30.2) domain of African green monkey TRIM5alpha determines species-specific restriction of simian immunodeficiency virus SIVmac infection. Journal of Virology 79: 8870–8877. doi: 10.1128/JVI.79.14.8870-8877.2005
View Article • PubMed/NCBI • Google Scholar

11. Hatziioannou T, Perez-Caballero D, Yang A, Cowan S, Bieniasz PD (2004) Retrovirus resistance factors Ref1 and Lv1 are species-specific variants of TRIM5alpha. Proceedings of the National Academy of Sciences of the United States of America 101: 10774–10779. doi: 10.1073/pnas.0402361101
View Article • PubMed/NCBI • Google Scholar

12. Keckesova Z, Ylinen LM, Towers GJ (2004) The human and African green monkey TRIM5alpha genes encode Ref1 and Lv1 retroviral restriction factor activities. Proceedings of the National Academy of Sciences of the United States of America 101: 10780–10785. doi: 10.1073/pnas.0402474101
View Article • PubMed/NCBI • Google Scholar

13. Perron MJ, Stremlau M, Song B, Ulm W, Mulligan RC, et al. (2004) TRIM5alpha mediates the postentry block to N-tropic murine leukemia viruses in human cells. Proceedings of the National Academy of Sciences of the United States of America 101: 11827–11832. doi: 10.1073/pnas.0403364101
View Article • PubMed/NCBI • Google Scholar

14. Nakayama EE, Shioda T (2010) Anti-retroviral activity of TRIM5 alpha. Rev Med Virol 20: 77–92. doi: 10.1002/rmv.637
View Article • PubMed/NCBI • Google Scholar

15. Song H, Nakayama EE, Yokoyama M, Sato H, Levy JA, et al. (2007) A single amino acid of the human immunodeficiency virus type 2 capsid affects its replication in the presence of cynomolgus monkey and human TRIM5alphas. Journal of Virology 81: 7280–7285. doi: 10.1128/JVI.00406-07
View Article • PubMed/NCBI • Google Scholar

16. Price AJ, Marzetta F, Lammers M, Ylinen LM, Schaller T, et al. (2009) Active site remodeling switches HIV specificity of antiretroviral TRIMCyp. Nat Struct Mol Biol 16: 1036–1042. doi: 10.1038/nsmb.1667
View Article • PubMed/NCBI • Google Scholar

17. Gamble TR, Yoo S, Vajdos FF, von Schwedler UK, Worthylake DK, et al. (1997) Structure of the carboxyl-terminal dimerization domain of the HIV-1 capsid protein. Science 278: 849–853. doi: 10.1126/science.278.5339.849
View Article • PubMed/NCBI • Google Scholar

18. Onyango CO, Leligdowicz A, Yokoyama M, Sato H, Song H, et al. (2010) HIV-2 capsids distinguish high and low virus load patients in a West African community cohort. Vaccine 28S2: B60–B67. doi: 10.1016/j.vaccine.2009.08.060
View Article • PubMed/NCBI • Google Scholar

19. Ibe S, Yokomaku Y, Shiino T, Tanaka R, Hattori J, et al. (2010) HIV-2 CRF01_AB: first circulating recombinant form of HIV-2. J Acquir Immune Defic Syndr 54: 241–247. doi: 10.1097/QAI.0b013e3181dc98c1
View Article • PubMed/NCBI • Google Scholar

20. Marlink R, Kanki P, Thior I, Travers K, Eisen G, et al. (1994) Reduced rate of disease development after HIV-2 infection as compared to HIV-1. Science 265: 1587–1590. doi: 10.1126/science.7915856
View Article • PubMed/NCBI • Google Scholar

21. Miyamoto T, Yokoyama M, Kono K, Shioda T, Sato H, et al. (2011) A single amino acid of human immunodeficiency virus type 2 capsid protein affects conformation of two external loops and viral sensitivity to TRIM5alpha. PloS one 6: e22779. doi: 10.1371/journal.pone.0022779
View Article • PubMed/NCBI • Google Scholar

22. Kono K, Song H, Shingai Y, Shioda T, Nakayama EE (2008) Comparison of anti-viral activity of rhesus monkey and cynomolgus monkey TRIM5alphas against human immunodeficiency virus type 2 infection. Virology 373: 447–456. doi: 10.1016/j.virol.2007.12.022
View Article • PubMed/NCBI • Google Scholar

23. Wu X, Anderson JL, Campbell EM, Joseph AM, Hope TJ (2006) Proteasome inhibitors uncouple rhesus TRIM5alpha restriction of HIV-1 reverse transcription and infection. Proceedings of the National Academy of Sciences of the United States of America 103: 7465–7470. doi: 10.1073/pnas.0510483103
View Article • PubMed/NCBI • Google Scholar

24. Anderson JL, Campbell EM, Wu X, Vandegraaff N, Engelman A, et al. (2006) Proteasome inhibition reveals that a functional preintegration complex intermediate can be generated during restriction by diverse TRIM5 proteins. Journal of Virology 80: 9754–9760. doi: 10.1128/JVI.01052-06
View Article • PubMed/NCBI • Google Scholar

25. Pertel T, Reinhard C, Luban J (2011) Vpx rescues HIV-1 transduction of dendritic cells from the antiviral state established by type 1 interferon. Retrovirology 8: 49. doi: 10.1186/1742-4690-8-49
View Article • PubMed/NCBI • Google Scholar

26. Sokolskaja E, Berthoux L, Luban J (2006) Cyclophilin A and TRIM5alpha independently regulate human immunodeficiency virus type 1 infectivity in human cells. Journal of Virology 80: 2855–2862. doi: 10.1128/JVI.80.6.2855-2862.2006
View Article • PubMed/NCBI • Google Scholar

27. Pertel T, Hausmann S, Morger D, Zuger S, Guerra J, et al. (2011) TRIM5 is an innate immune sensor for the retrovirus capsid lattice. Nature 472: 361–365. doi: 10.1038/nature09976
View Article • PubMed/NCBI • Google Scholar

28. Kono K, Song H, Yokoyama M, Sato H, Shioda T, et al. (2010) Multiple sites in the N-terminal half of simian immunodeficiency virus capsid protein contribute to evasion from rhesus monkey TRIM5alpha-mediated restriction. Retrovirology 7: 72. doi: 10.1186/1742-4690-7-72
View Article • PubMed/NCBI • Google Scholar

29. Pornillos O, Ganser-Pornillos BK, Kelly BN, Hua Y, Whitby FG, et al. (2009) X-ray structures of the hexameric building block of the HIV capsid. Cell 137: 1282–1292. doi: 10.1016/j.cell.2009.04.063
View Article • PubMed/NCBI • Google Scholar

30. Ganser-Pornillos BK, Yeager M, Sundquist WI (2008) The structural biology of HIV assembly. Curr Opin Struct Biol 18: 203–217. doi: 10.1016/j.sbi.2008.02.001
View Article • PubMed/NCBI • Google Scholar

31. Inagaki N, Takeuchi H, Yokoyama M, Sato H, Ryo A, et al. (2010) A structural constraint for functional interaction between N-terminal and C-terminal domains in simian immunodeficiency virus capsid proteins. Retrovirology 7: 90. doi: 10.1186/1742-4690-7-90
View Article • PubMed/NCBI • Google Scholar

32. Bailey GD, Hyun JK, Mitra AK, Kingston RL (2012) A structural model for the generation of continuous curvature on the surface of a retroviral capsid. J Mol

Biol 417: 212–223. doi: 10.1016/j.jmb.2012.01.014
View Article • PubMed/NCBI • Google Scholar

33. Gao F, Yue L, White AT, Pappas PG, Barchue J, et al. (1992) Human infection by genetically diverse SIVSM-related HIV-2 in west Africa. Nature 358: 495–499. doi: 10.1038/358495a0
View Article • PubMed/NCBI • Google Scholar

34. Hillis DM, Bull JJ (1993) An empirical test of bootstrapping as a method for assessing confidence in phylogenetic analysis. Syst Biol 42: 182–192.
View Article • PubMed/NCBI • Google Scholar

35. Pear WS, Nolan GP, Scott ML, Baltimore D (1993) Production of high-titer helper-free retroviruses by transient transfection. Proc Natl Acad Sci U S A 90: 8392–8396. doi: 10.1073/pnas.90.18.8392
View Article • PubMed/NCBI • Google Scholar

36. Lasfargues EY, Lasfargues JC, Dion AS, Greene AE, Moore DH (1976) Experimental infection of a cat kidney cell line with the mouse mammary tumor virus. Cancer Res 36: 67–72.
View Article • PubMed/NCBI • Google Scholar

37. Sheehy AM, Gaddis NC, Choi JD, Malim MH (2002) Isolation of a human gene that inhibits HIV-1 infection and is suppressed by the viral Vif protein. Nature 418: 646–650. doi: 10.1038/nature00939
View Article • PubMed/NCBI • Google Scholar

38. Dodson GG, Lane DP, Verma CS (2008) Molecular simulations of protein dynamics: new windows on mechanisms in biology. EMBO Rep 9: 144–150. doi: 10.1038/sj.embor.7401160
View Article • PubMed/NCBI • Google Scholar

39. Baker D, Sali A (2001) Protein structure prediction and structural genomics. Science 294: 93–96. doi: 10.1126/science.1065659
View Article • PubMed/NCBI • Google Scholar

40. Shirakawa K, Takaori-Kondo A, Yokoyama M, Izumi T, Matsui M, et al. (2008) Phosphorylation of APOBEC3G by protein kinase A regulates its interaction with HIV-1 Vif. Nat Struct Mol Biol 15: 1184–1191. doi: 10.1038/nsmb.1497
View Article • PubMed/NCBI • Google Scholar

41. Case DA, Darden TA, Cheatham I, T.E., Simmerling CL, Wang JR, et al.. (2006) AMBER 9. University of California, San Francisco.

42. Hornak V, Abel R, Okur A, Strockbine B, Roitberg A, et al. (2006) Comparison of multiple Amber force fields and development of improved protein backbone parameters. Proteins 65: 712–725. doi: 10.1002/prot.21123
View Article • PubMed/NCBI • Google Scholar

43. Ryckaert J-P, Ciccotti G, Berendsen HJC (1977) Numerical integration of the cartesian equations of motion of a system with constraints: Molecular dynamics of n-alkanes. J Comput Phys 23: 327–341. doi: 10.1016/0021-9991(77)90098-5
View Article • PubMed/NCBI • Google Scholar

44. Ponder JW, Case DA (2003) Force fields for protein simulations. Adv Protein Chem 66: 27–85. doi: 10.1016/s0065-3233(03)66002-x
View Article • PubMed/NCBI • Google Scholar

45. Lee K, Chu CK (2001) Molecular modeling approach to understanding the mode of action of L-nucleosides as antiviral agents. Antimicrob Agents Chemother 45: 138–144. doi: 10.1128/AAC.45.1.138-144.2001
View Article • PubMed/NCBI • Google Scholar

46. Kinomoto M, Yokoyama M, Sato H, Kojima A, Kurata T, et al. (2005) Amino acid 36 in the human immunodeficiency virus type 1 gp41 ectodomain controls fusogenic activity: implications for the molecular mechanism of viral escape from a fusion inhibitor. Journal of Virology 79: 5996–6004. doi: 10.1128/JVI.79.10.5996-6004.2005
View Article • PubMed/NCBI • Google Scholar

nature
structural &
molecular biology

The APOBEC3C crystal structure and the interface for HIV-1 Vif binding

Shingo Kitamura[1,2], Hirotaka Ode[1], Masaaki Nakashima[1,2], Mayumi Imahashi[1,3], Yuriko Naganawa[1], Teppei Kurosawa[1,2], Yoshiyuki Yokomaku[1], Takashi Yamane[2], Nobuhisa Watanabe[2,4], Atsuo Suzuki[2], Wataru Sugiura[1,3] & Yasumasa Iwatani[1,3]

The human apolipoprotein B mRNA-editing enzyme catalytic polypeptide–like 3 (APOBEC3, referred to as A3) proteins are cellular cytidine deaminases that potently restrict retrovirus replication. However, HIV-1 viral infectivity factor (Vif) counteracts the antiviral activity of most A3 proteins by targeting them for proteasomal degradation. To date, the structure of an A3 protein containing a Vif-binding interface has not been solved. Here, we report a high-resolution crystal structure of APOBEC3C and identify the HIV-1 Vif–interaction interface. Extensive structure-guided mutagenesis revealed the role of a shallow cavity composed of hydrophobic or negatively charged residues between the α2 and α3 helices. This region is distant from the DPD motif (residues 128–130) of APOBEC3G that participates in HIV-1 Vif interaction. These findings provide insight into Vif-A3 interactions and could lead to the development of new pharmacologic anti–HIV-1 compounds.

The A3 family of cytidine deaminases consists of cellular proteins that prevent the mobilization of diverse retroviruses, retrotransposons and other viral pathogens (reviewed in ref. 1). In humans, seven members of this protein family, A3A, A3B, A3C, A3DE, A3F, A3G and A3H, are encoded in a tandem array on chromosome 22 (ref. 2). The A3 proteins are characterized by the presence of one or two conserved zinc-coordinating domains (Z domains) consisting of $HXE(X)_{23-28}CXXC$ motifs (reviewed in ref. 3). On the basis of phylogenetic analyses, the Z domains fall into three types: Z1 (A3A and the C-terminal domains (CTDs) of A3B and A3G), Z2 (A3C, both halves of A3DE and A3F, and the N-terminal domains (NTDs) of A3B and A3G) and Z3 (A3H)[2]. The Z2 domain can be further subdivided into three subgroups on the basis of amino acid sequences: the A3F NTD (the NTDs of A3B, A3DE and A3F), the A3G NTD and the A3F CTD (A3C and the CTDs of A3DE and A3F) subgroups.

HIV-1 Vif protein overcomes the antiviral activity of A3 proteins in infected cells by forming an E3 ubiquitin ligase complex, with cullin 5, elongin B (EloB) and elongin C (EloC) in collaboration with core-binding factor β (CBF-β)[4,5], which subsequently leads to A3 degradation through the ubiquitin-proteasome pathway[6–8]. Thus, the elimination of A3 in cells during virus production prevents its encapsidation into progeny HIV-1 viruses. A3 degradation specificity is determined by the ability of Vif to bind to the target. HIV-1 Vif binds A3C, A3DE, A3F, A3G and A3H but not A3A and A3B. Among the Z domains, only Z3 (A3H haplotype II) and Z2 (the A3G NTD and the A3F CTD subgroups) contain a critical interface that interacts with HIV-1 Vif[9–11].

One specific residue of the human A3G NTD responsible for the Vif interaction, Asp128, was primarily identified by comparative studies of species-specific A3G-Vif interactions[12–15]. Subsequently, extensive mutational analyses of amino acids adjacent to Asp128 revealed that the 128-Asp-Pro-Asp-130 (DPD) motif of A3G, located at loop 7 between β4 and α4, is crucial for the direct interaction with Vif[16]. These critical residues in the A3G NTD have been mapped to a variable-loop structure in close proximity to the nucleic acid–binding surface. In contrast, two independent studies have reported that two residues that are critical for the Vif interaction, Glu289 and Glu324 of the A3F CTD, are situated in the α3 and α4 helices, respectively, which are located distally from the DPD motif[10,17]. Despite our knowledge of these critical A3 residues, the structural features underlying the Vif-interaction interface on A3 proteins have not been previously elucidated.

To date, the three-dimensional structure of only the A3G CTD has been determined by NMR[18,19] or X-ray crystallography[20,21]. The structures of full-length A3 or the domain involved in the HIV-1 Vif–binding interface have not been previously solved. Here, we present the first report, to our knowledge, of the crystal structure of full-length human A3C. We used extensive structure-guided mutagenesis to explore the residues that form the HIV-1 Vif–binding interface. Our results demonstrate that ten residues of A3C are critical for the formation of the Vif-interaction interface, which mapped to a different region from loop 7 that corresponds to an area of the DPD motif in the A3G NTD. Furthermore, our data indicate that the responsible interface provides a shallow cavity composed of hydrophobic or

[1]Clinical Research Center, Department of Infectious Diseases and Immunology, National Hospital Organization Nagoya Medical Center, Nagoya, Japan. [2]Department of Biotechnology, Graduate School of Engineering, Nagoya University, Nagoya, Japan. [3]Program in Integrated Molecular Medicine, Graduate School of Medicine, Nagoya University, Nagoya, Japan. [4]Synchrotron Radiation Research Center, Nagoya University, Nagoya, Japan. Correspondence should be addressed to Y.I. (iwataniy@nnh.hosp.go.jp).

Received 23 April; accepted 7 August; published online 23 September 2012; doi:10.1038/nsmb.2378

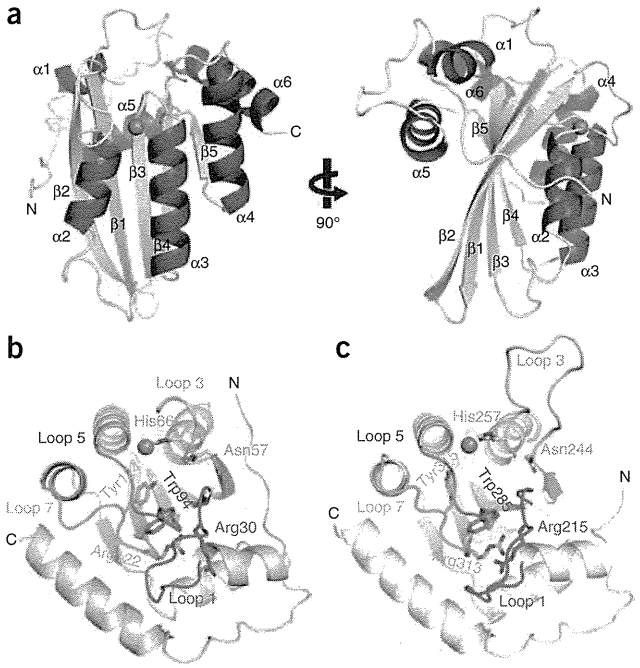

Figure 1 The X-ray crystal structure of full-length A3C. (**a**) Two views of the A3C structure, rotated by 90°, are shown. The α-helices (α1–α6) and β-strands (β1–β5) are colored in red and yellow, respectively. A coordinated zinc ion is represented as a blue sphere. (**b**,**c**) Structural comparison around the catalytic groove of A3C (**b**) and A3G CTD (**c**). Amino acid side chains of the conserved residues in loop 1 (magenta), loop 3 (yellow), loop 5 (orange) and loop 7 (cyan) are labeled with the residue numbers.

negatively charged residues. In addition, we found that the structural features of the Vif-binding interfaces are conserved in the homologous Z2-type A3C, A3F and A3DE proteins but not in the A3G protein. These results will deepen our understanding of A3-Vif interactions and aid in the development of new strategies using potential endogenous inhibitors against HIV-1.

RESULTS

High-resolution crystal structure of full-length A3C

Initially, human A3C was expressed in *Escherichia coli* as an N-terminal GST-tagged recombinant protein to increase its solubility. The tag was subsequently removed. We further purified the full-length A3C protein (residues 1–190) and solved its structure at 2.15 Å (**Fig. 1a** and **Table 1**). The A3C structure has a core platform composed of six α-helices (α1–α6) and five β-strands (β1–β5), with a coordinated zinc ion that is well conserved in the cytidine deaminase superfamily[22]. The superimposition of the A3C core onto that of the A3G CTD crystal structure (PDB 3IR2) for 86% of the backbone atoms exhibited a Cα r.m.s. deviation of 1.36 Å, thereby indicating the structural conservation of the core platform.

In contrast to the high conservation of the core structures, the loop regions, particularly loops 1, 3, 4 and 7 of the A3C and A3G CTD structures, are distinct (**Fig. 1b**,**c** and **Supplementary Fig. 1a**,**b**). Nevertheless, the positions of certain residues in the loops exhibit structural similarity. Arg30, Asn57, His66, Trp94, Arg122 and Tyr124 in A3C (**Fig. 1b**) are similar to Arg215, Asn244, His257, Trp285, Arg313 and Tyr315 in the A3G CTD (**Fig. 1c**). These residues primarily have critical roles in maintaining the conformation of the catalytic center and the groove involved in substrate binding[18,20], which are functionally conserved features among A3 proteins. In contrast, differences in the HIV-1 Vif interaction are attributable to unique conformational differences between the A3C and A3G CTD structures.

Notably, the A3C structure exhibits a continuous well-ordered β2-strand that is remarkably different from that of the A3G CTD (PDB 3IR2) (**Fig. 1** and **Supplementary Fig. 1a**,**b**). Molecular dynamics (MD) simulations support the high stability of the A3C β2 (**Supplementary Fig. 1c–f**), which is also observed in the APOBEC2 (A2) crystal structure[23]. In the A2 structure, a continuous β2 strand mediates dimerization through a β2 of another molecule. However, we did not detect any intermolecular contacts through the β2-β2 interaction within the 20 largest contacts in the crystal packing (**Supplementary Fig. 2a**). In addition, our dynamic light-scattering experiments indicated both monomodal and bimodal distributions of A3C proteins in solution (**Supplementary Fig. 2b**), although our gel-filtration data indicated that most of the protein was distributed in the monomer size fraction (**Supplementary Fig. 2c**). These results suggest that dynamic A3C dimerization might occur but not through their β2 strands. This effect might be partly owing to 13 amino acids of the N-terminal region, which reside on the β2 strand, that sterically hinder the β2-β2 associations. Recently, a similar observation with a full-length A2 structure has also been reported[24].

Ten A3C residues are critical for HIV-1 Vif binding

To determine the interface for HIV-1 Vif recognition of A3C, extensive structure-guided mutagenesis experiments were performed by using an approach analogous to that previously described for A3G[25]. A single

Table 1 Data collection and refinement statistics

	APOBEC3C
Data collection	
Space group	$P6_1$
Cell dimensions	
a, *b*, *c* (Å)	105.04, 105.04, 70.05
α, *β*, *γ* (°)	90, 90, 120
Resolution (Å)	105–2.15 (2.19–2.15)
R_{merge}	5.4 (33.8)
$I / \sigma I$	94.5 (13.3)
Completeness (%)	99.9 (100)
Redundancy	22.3 (22.6)
Refinement	
Resolution (Å)	91–2.15
No. reflections	22,783
R_{work} / R_{free}	21.4 / 26.3
No. atoms	3,281
Protein	3,188
Ligand/ion	3
Water	90
B factors	45.56
Protein	45.69
Ligand/ion	45.50
Water	40.90
R.m.s. deviations	
Bond lengths (Å)	0.012
Bond angles (°)	1.390

A single crystal was used for solving the structure. Values in parentheses are for highest-resolution shell.

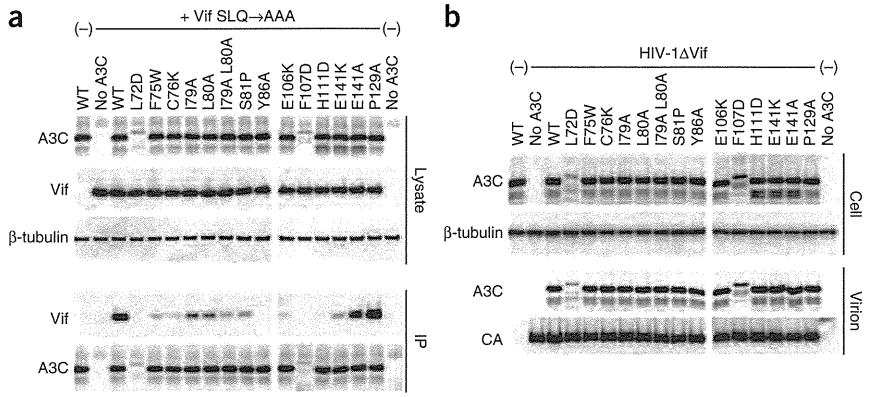

Figure 2 Ten A3C residues critical for HIV-1 Vif interaction. (**a**) Immunoblots of lysates and anti-His immunoprecipitates of HEK-293T cells with wild type (WT), mutant A3C-Myc-His or control plasmid (no A3C) expressed in the presence (+) or absence (–) of HIV-1 Vif SLQ→AAA. Immunoblotting is with anti-Vif or anti-His monoclonal antibodies as shown. Anti–β-tubulin antibody was used as a loading control. IP, immunoprecipitation. (**b**) Virion-packaging efficiency of Vif-resistant A3C mutants. Intracellular (cell) and virus-incorporated (virion) levels of A3C WT and mutants analyzed by western blotting. Samples are from cells transfected with HIV-1ΔVif or control plasmids (–), plus either A3C or control plasmids (no A3C). The HIV-1 capsid protein (CA) levels in virions were detected with an anti-p24 antibody.

E106K substitution changes the susceptibility of A3C to Vif-mediated degradation[10], which suggests that Glu106 is one of the residues responsible for the A3C-Vif interaction. Therefore, to further identify the other critical residues adjacent to Glu106, we first introduced substitution mutations near Glu106 and tested the Vif sensitivity *in vitro*. The results are summarized in **Supplementary Figure 3**. Wild-type A3C was not detectable when coexpressed with Vif (Vif sensitive), whereas the expression of the E106K mutant was unchanged in the presence of Vif (Vif resistant). These experiments were repeated for all residues whose mutations resulted in a Vif-resistant phenotype, until the surrounding A3C surface residues were all associated with sensitive mutants. The percentage reduction of A3C expression in the presence relative to the absence of Vif was evaluated (Vif-resistance level) (**Supplementary Fig. 3**). The results indicated that any single point mutation in the nine residues (Leu72, Phe75, Cys76, Ile79, Leu80, Ser81, Tyr86, Glu106 and Phe107) resulted in a >50% Vif-resistance level, whereas the mutations H111D and A109K resulted in 45% and 41% resistance, respectively. To evaluate whether these residues were intrinsically involved in the Vif interaction, we immunoprecipitated a Vif SOCS-box mutant (Vif SLQ→AAA) that can bind A3 but not EloBC[8,26,27] in the presence of wild-type or Myc-His-tagged A3C mutants, and immunoblotted for Vif SLQ→AAA (**Fig. 2a**). Vif was coimmunoprecipitated with wild-type A3C and A3C P129A at equal levels (**Fig. 2a**), which indicated that Pro129 in A3C is not responsible for the Vif interaction, unlike findings with A3G[16]. In contrast, all of the Vif-resistant A3C mutants immunoprecipitated minimal amounts of Vif, which indicated that the residues whose mutations conferred the Vif-resistant phenotypes are indeed critical for the Vif interaction. The E141K mutation abolished Vif binding, despite being relatively Vif sensitive. The reason for this effect is not clear. These findings demonstrated that Leu72, Phe75, Cys76, Ile79, Leu80, Ser81, Tyr86, Glu106, Phe107 and His111 are involved in forming the Vif-interaction interface. All of the binding-deficient A3C mutants were incorporated into *vif*-deficient HIV-1 (HIV-1ΔVif) as efficiently as wild-type A3C (**Fig. 2b**), which suggested that RNA-binding capacity was not impaired by the A3C mutations.

Structural mapping of the mutagenesis results yielded a Vif-resistance level, which is color-coded on the structure (**Fig. 3a,b**). The residues involved in the Vif interaction are located in an area between the α2 and α3 helices, distal from the Pro129 of the A3G DPD motif[16]. Notably, in the A3C surface representation, the interface is a shallow cavity composed of hydrophobic (Leu72, Ile79 and Leu80) or aromatic (Phe75, Tyr86, Phe107 and His111) residues at the bottom and hydrophilic (Cys76, Ser81 and Glu106) residues at the edges (**Fig. 3a–c**). One notable feature of this cavity is that two potential π interactions can be observed at the bottom, on the basis of the configuration of four aromatic residues (Phe75, Tyr86, Phe107

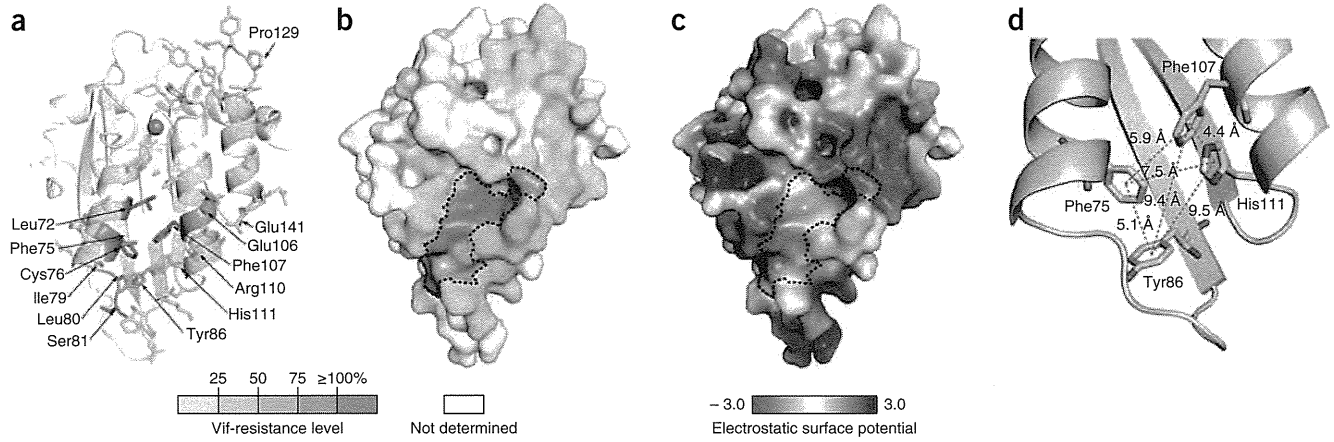

Figure 3 The A3C interface for the HIV-1 Vif interaction. (**a**,**b**) The A3C structure, displaying critical residues for Vif sensitivity. The residues are colored in the ribbon (**a**) and surface (**b**) representations of A3C according to the resistance level of Vif-mediated degradation, as shown in the bottom bar. Residues exhibiting a >50% Vif-resistance level are enclosed by a dotted line. (**c**) The electrostatic potential of A3C is shown. The accessible surface area is colored according to the calculated electrostatic potential from –3 *kT/e* (red) to 3 *kT/e* (blue). The orientation and the dotted line are the same as in **b**. (**d**) Potential π-stacking interactions at the Vif-binding interface in A3C. The distances between the four aromatic residues involved in the Vif-binding cavity (Phe75, Tyr86, Phe107 and His111) are shown.

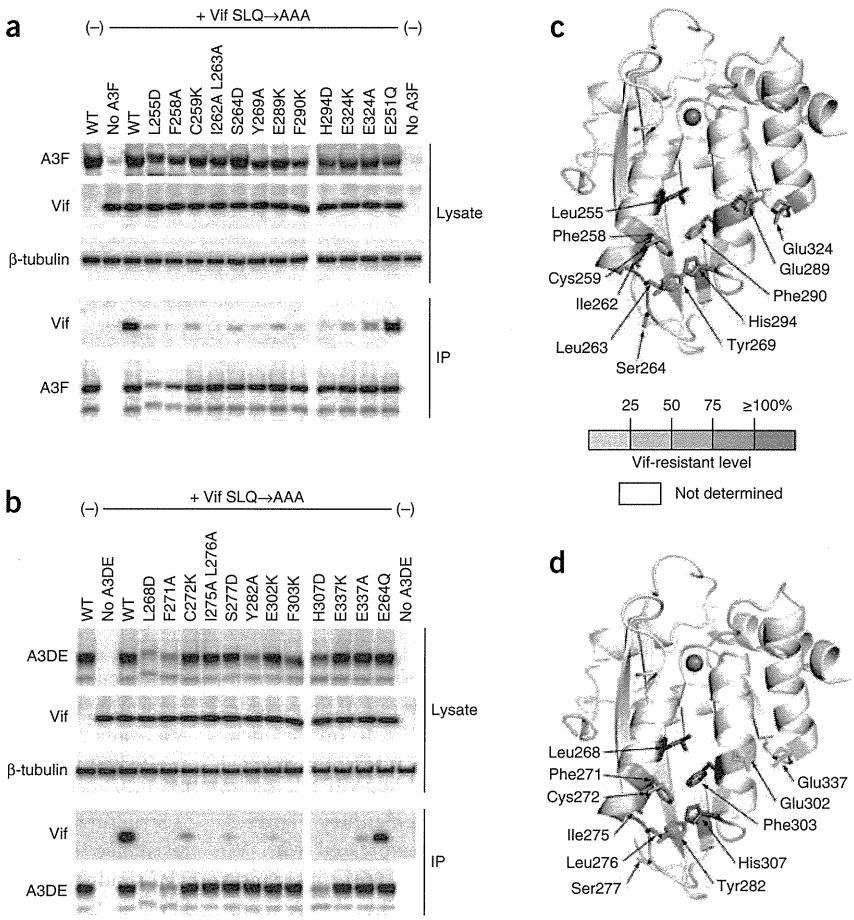

Figure 4 Analogous residues of A3F and A3DE are involved in the HIV-1 Vif-binding interface. (**a**,**b**) Coimmunoprecipitation (IP) of HIV-1 Vif SLQ→AAA with wild type (WT) or A3F-MycHIS mutants (**a**) and with wild type or A3DE-MycHIS mutants (**b**). (**c**,**d**) Residues are mapped on the A3F (**c**) or the A3DE CTD (**d**) structures modeled on the A3C crystal structure. The residues are color coded according to their Vif-resistance levels. A coordinated zinc ion is shown as a blue sphere.

and His111) (**Fig. 3d**). Both Phe75-Tyr86 and Phe107-His111 show the proper distance and orientation to make two weak π-π interactions. In contrast, the pair of Phe75-Phe107 shows theoretically proper distance, although the angle is not appropriate to form a potential interaction. In addition, because a mutation of the hydrophobic or aromatic residues disrupts the Vif interaction and subsequent degradation, a specific size of the hydrophobic side chains, as well as π stacking, may be important for maintaining the correct interface conformation and for the A3C-Vif interaction. The interface includes a flexible region, loop 4, where Cys76, Ile79, Leu80 and Ser81 exhibit higher temperature factors in the crystal-structure data and in the MD simulations (**Supplementary Fig. 1f**), which suggests a partially flexible interface. Furthermore, the electrostatic surface potential analysis revealed a negatively charged interface (**Fig. 3c**), and substitutions with positively charged residues increase the Vif-resistance levels (**Supplementary Fig. 3**), which suggests that the negative electrostatic surface at the interface is also an important feature for HIV-1 Vif binding.

Vif-binding interfaces are conserved in A3C, A3F and A3DE

We also performed analogous coimmunoprecipitation experiments with equivalent mutations in the A3F and A3DE CTDs and tested for Vif interaction (**Fig. 4**). For A3F, involvement of the A3F Glu289 and Glu324 residues in Vif interaction has been reported[10,17]. Coimmunoprecipitates of these A3F mutants contained significantly reduced amounts of Vif (**Fig. 4a**) compared to wild type or E251Q (a mutation at the catalytic center), which demonstrates that the equivalent residues of A3F, Leu255, Phe258, Cys259, Ile262, Leu263, Ser264, Tyr269, Glu289, Phe290 and His294, are also important for the Vif interaction. In addition, we assessed the Vif sensitivity of the mutants (**Supplementary Fig. 3c**,**e**) and mapped the residues onto a homology model of the A3F CTD (**Fig. 4c**). Again, these residues were clustered and formed a Vif-binding cavity homologous to that observed in the A3C structure, although a slight difference in the Vif-resistant phenotype was observed. The E141K A3C mutant displayed a low Vif-resistance level (27%), whereas the corresponding A3F mutant, E324K, had a high resistance level (87%) (**Supplementary Fig. 3c**,**e**). MD simulations suggested that conformational differences at the negatively charged edge of the cavity may be responsible for these differences (**Supplementary Fig. 4**).

For A3DE, the analysis of the coimmunoprecipitation assays demonstrated that 10 equivalent residues (Leu268, Phe271, Cys272, Ile275, Leu276, Ser277, Tyr282, Glu302, Phe303 and His307) of A3DE are also important for Vif interaction (**Fig. 4b**). In addition, mutations at any of the residues critical for Vif interaction resulted in a Vif-resistant phenotype, although the A3DE S277D and E302K mutants presented a lower of the Vif-resistance than the equivalents of A3F S264D and E289K, respectively (**Supplementary Fig. 3c–f**). Moreover, these residues provide a similar Vif-binding interface to that of A3C (**Fig. 4d**). These results suggest that the conformation of the Vif-interaction interface is highly conserved among A3C and the CTDs of A3F and A3DE.

To further assess whether the Z2-type A3G NTD provides a similar Vif-interaction interface at the equivalent position between the α2 and α3 helices, we constructed four analogous A3G mutants, F74W, L80D, Y86A and F107K, that have a substitution at identical residues, on the basis of sequence alignments between A3C and the A3G NTD. Examination of Vif sensitivity in these mutants indicated that none of these mutations in the A3G NTD changed the Vif-sensitive phenotype (**Supplementary Fig. 5**). These results demonstrated that the Vif-binding interface of A3G NTD is distinct from that of A3C, A3F and A3DE. In addition, they suggest that mutations between the α2 and α3 helices do not distort the presumed Vif-binding interface conformation of the A3G NTD.

Vif-resistant A3F inhibits HIV-1 infection

To elucidate the effects of the A3F mutations on viral incorporation, we analyzed the amounts of wild-type and mutant A3F proteins in cells and virions. Both wild-type and mutant A3F were efficiently incorporated into virus particles, with the exception of the H294D

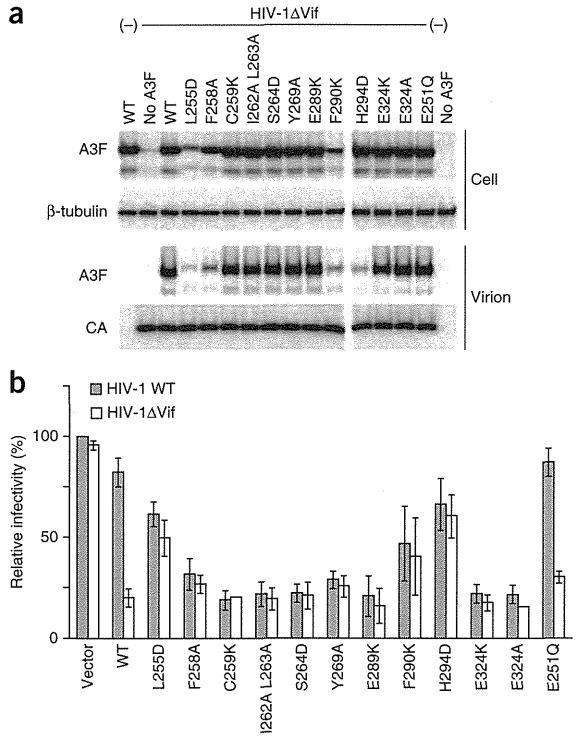

Figure 5 The effects of mutations at the equivalent residues in A3F on antiviral activity. (**a**) Intracellular expression (cell) and incorporation of wild-type A3F and the mutants into virions (virion), evaluated by western blotting. The CA level in virions was detected by an anti-p24 antibody. (**b**) The antiviral effects of A3F and mutants on wild-type HIV-1 (HIV-1 WT) or HIV-1ΔVif in a single-round replication assay with LuSIV cells. The relative viral infectivity of wild-type HIV-1 in the absence of A3F (vector) was set to 100%. Relative infectivity data are shown as means ± s.d. of three independent experiments.

mutant (**Fig. 5a**). This result suggests that the critical residues for Vif interaction (except for His294) of A3F are not located in the region that is responsible for A3F packaging into virions. Finally, to evaluate whether the A3F mutants exhibited any antiviral activity against HIV-1, we compared the infectivity of wild-type HIV-1 and HIV-1ΔVif in the presence of wild-type or mutant A3F. The wild-type A3F and the E251Q mutant reduced HIV-1ΔVif infectivity to 21% and 30%, respectively, whereas wild-type HIV-1 infectivity was only marginally affected (**Fig. 5b**). In contrast, all of the Vif-resistant A3F mutants suppressed the infectivity of wild-type HIV-1 as efficiently as for HIV-1ΔVif, which is consistent with their packaging level (**Fig. 5a,b**). These findings demonstrate that a disruption of the A3F-Vif interaction prevents A3F degradation and thereby allows A3F to be efficiently packaged into HIV-1 virions to exert its antiviral activity.

DISCUSSION

Studies conducted over the past decade have established that HIV-1 Vif abolishes the antiviral activity of A3 by recruiting an E3 ubiquitin ligase complex to promote proteasomal degradation. Many efforts toward developing strategies that interfere with the A3-Vif interaction have been unsuccessful to date, in part because of the lack of available structural information on the A3-Vif interaction interface. Here, we present, to our knowledge, the first crystal structure of A3C containing an HIV-1 Vif-interaction interface. In addition, our extensive structure-guided mutagenesis revealed the precise Vif-interaction site, between the α2 and α3 helices of A3C, and permitted the delineation of structural features (negatively charged, hydrophobic and partially flexible) in the Vif-interaction interface. Additional investigations demonstrated that the Vif-binding interfaces are highly conserved among Z2-type cytidine deaminases, including A3C, A3F and A3DE, but not A3G.

In combination with the A3C structure, our results suggest that the Vif-interaction interface forms a shallow cavity that is composed of hydrophobic and negatively charged residues. Notably, the positively charged DRMR motif (residues 14–17)[26] and hydrophobic residues (Leu24, Val25, Leu64, Ile66 and Leu72) on HIV-1 Vif are required for its specific interaction with A3C (reviewed in ref. 28), thereby confirming that both the electrostatic and hydrophobic interactions are the fundamental driving force for the A3C-Vif interaction. In addition, Vif Trp5, Trp21, Trp38, Tyr69, Trp70 and Trp89 are commonly considered essential for the interaction with A3C, A3F, A3DE or A3G. These data suggest that the π interactions of the aromatic residues between the A3C interface and Vif may contribute to their association, and these interactions are presumably common to all A3-Vif interactions. Recent reports indicate that Vif Trp21 and Trp38 are important for binding with the cofactor CBF-β. The π interactions may be mediated by CBF-β for efficient formation of the E3 ubiquitin ligase complex[4,5,29]. In addition, the existence of a partially flexible region in the Vif-binding interface (**Supplementary Fig. 1f**) suggests that the cavity may not locally exhibit a fixed conformation, and certain structural changes may be induced by Vif to allow a tight interaction.

Although the A3G NTD is categorized as a Z2-type cytidine deaminase, the amino acid sequences of the A3G NTD and A3C are quite different; only 42.8% of the A3C sequences are identical to the A3G NTD, whereas 77% and 76% are identical to the A3F CTD and A3DE CTD sequences, respectively. In particular, the residues of the α2–α3 regions are not homologous between A3C, A3F, A3DE and the A3G NTD, which suggests differences in their local conformations. For A3C, the Vif-binding interface is located in a region distal to loop 7 that corresponds to an area of the DPD motif in the A3G NTD. In addition, our homologous mutagenesis showed that the equivalent area of the A3G NTD between the α2 and α3 helices is not critical for the A3G-Vif interaction (**Supplementary Fig. 5**), demonstrating that two different regions in A3C and the A3G NTD molecules participate in each specific interaction with Vif. The presence of these distinct interfaces is consistent with the evidence that the HIV-1 Vif residues responsible for binding to A3 proteins are different. The YRHHY motif (residues 40–44) and the DRMR motif in Vif are involved in specific interactions with A3G, and A3C, A3F or A3DE, respectively[11,26,30–33]. Nevertheless, because both types of A3-Vif interactions fundamentally require electrostatic and hydrophobic bindings and the involvement of the flexible loop conformations (loop 4 for A3C, A3F or A3DE; loop 7 for A3G), the interfaces of A3C, A3F or A3DE and A3G may have similar structural characteristics.

Our determination of the high-resolution A3C crystal structure and extensive structure-guided mutagenesis revealed the A3C structural features associated with the Vif interaction. In addition, the conformation of the Vif-binding interface is highly conserved within the Z2-type A3 subfamily. The location of the Vif-binding interface on A3 proteins may prove to be important during the development of pharmacologic agents that target A3-Vif interactions. Previous reports have shown that the residues of A3G and A3C that are critical for nucleic acid binding also have essential roles in the efficient packaging